Journal of Coastal Research	33	3	487–506	Coconut Creek, Florida	May 2017

Shoreline and Sand Storage Dynamics from Annual Airborne LIDAR Surveys, Texas Gulf Coast

Jeffrey G. Paine*, Tiffany L. Caudle, and John R. Andrews

Bureau of Economic Geology
John A. and Katherine G. Jackson School of Geosciences
The University of Texas at Austin
Austin, TX 78758, U.S.A.

www.cerf-jcr.org

www.JCRonline.org

ABSTRACT

Paine, J.G.; Caudle, T.L., and Andrews, J.R., 2017. Shoreline and sand storage dynamics from annual airborne LIDAR surveys, Texas Gulf Coast. *Journal of Coastal Research,* 33(3), 487–506. Coconut Creek (Florida), ISSN 0749-0208.

Annual airborne LIDAR surveys were conducted along the Texas Gulf of Mexico shoreline between 2010 and 2012 to map shoreline position, determine shoreline movement and its historical context, and quantify beach and dune morphology by determining elevation threshold area (ETA) relationships for Holocene barrier islands, strandplains, and fluvial and deltaic headlands and marshes. Historical (1800s to 2007) movement is erosional for all major Texas shoreline segments, averaging 1.3 m/y of retreat. Shorelines retreated between 2007 and 2010 at a higher average rate of 2.8 m/y because of erosion and partial recovery from Hurricanes Ike (2008), Humberto (2007), and Dolly (2008). Despite the erosional context, airborne LIDAR surveys show that the shoreline advanced at 75% of 11,783 monitoring sites between 2010 and 2011 and moved an average of 6.5 m seaward during storm recovery. The recovery reversed between 2011 and 2012, when the shoreline retreated at 67% of 11,811 sites and moved an average of 3.1 m landward. Movement was similar to historical trends: NE and southern coast shorelines retreated, whereas central coast shorelines were relatively stable. Retreat between 2011 and 2012 did not fully offset advance between 2010 and 2011; the shoreline advanced at 59% of 11,811 sites and moved an average of 3.4 m seaward between 2010 and 2012, resulting in a net area gain of 203 ha. LIDAR-derived beach and dune areas exceeding threshold elevations of 2–9 m above mean sea level (at 1-m increments), divided by shoreline length over which the ETAs were determined, were used to produce average profiles. These data can be used to determine sediment storage volumes and temporal change, flood susceptibility, and erosion resilience. Storage patterns evident in ETA data mimic historical shoreline movement. Low elevation and sand storage occur where retreat is highest, whereas higher elevation and storage occur where retreat is lowest.

ADDITIONAL INDEX WORDS: *Coastal change, sediment budget, beach profiles, storm erosion and recovery.*

INTRODUCTION

The Gulf of Mexico (Gulf) beach and dune system on the Texas coast (Figure 1) is a dynamic geologic environment. Shoreline position and beach and dune morphology (height, width, and change over time) are critical parameters that respond to the balance among several important processes, including sea-level rise, land subsidence, sediment influx, littoral drift, and storm frequency, intensity, and recovery. Because the Texas coast faces continued developmental pressure as the coastal population rises, analysis of short- and long-term Gulf coastal change can serve as a planning tool to identify areas of habitat gain or loss; better quantify erosion and storm flooding threats to residential, industrial, and recreational facilities and transportation infrastructure; and help understand the natural and anthropogenic causes of beach, dune, and vegetation change. Periodic analyses of shoreline and dune morphology, rates of change, and contributing factors give citizens, organizations, planners, and regulators an indication of the current status of the coast and help determine whether change is accelerating, decelerating, or continuing at the same rate. This study examines annual-scale shoreline and beach and dune morphological change from repeat airborne LIDAR surveys of the Texas Gulf shoreline in 2010, 2011, and 2012 and places short-term shoreline movement in a longer-term (historical) context.

The Texas Gulf shoreline forms the seaward boundary along a series of Holocene geomorphic features (Figure 1) that include barrier islands, strandplains, fluvial and deltaic headlands, and chenier plains (Aronow *et al.*, 1982; Brown, Brewton, and McGowen, 1975; Brown *et al.*, 1975, 1976; LeBlanc and Hodgson, 1959). Three major rivers, including the Brazos and Colorado on the upper (NE) Texas coast and the Rio Grande on the lower (southern) Texas coast, directly discharge into the Gulf of Mexico, although their contribution to the overall coastal sediment budget has diminished with the construction of dams for flood control, water supply, and recreation in each river basin in the 20th century. Coastal embayments such as Galveston Bay formed landward of the Holocene barrier islands and peninsulas in late Pleistocene river valleys submerged during the Holocene transgression (LeBlanc and Hodgson, 1959), and shore-parallel lagoons such as Laguna Madre and E Matagorda Bay formed as barrier islands and peninsulas aggraded and expanded laterally along the coast. Tidal exchange between the bays, lagoons, and Gulf occurs through tidal passes and channels at Sabine Pass, Rollover Pass, Bolivar Roads, San Luis Pass, Brown Cedar Cut, Pass Cavallo, Cedar Bayou, Aransas Pass, Packery Channel, Mansfield Channel, and Brazos Santiago

DOI: 10.2112/JCOASTRES-D-15-00241.1 received 19 December 2015; accepted in revision 4 May 2016; corrected proofs received 20 July 2016; published pre-print online 22 September 2016.
*Corresponding author: jeff.paine@beg.utexas.edu

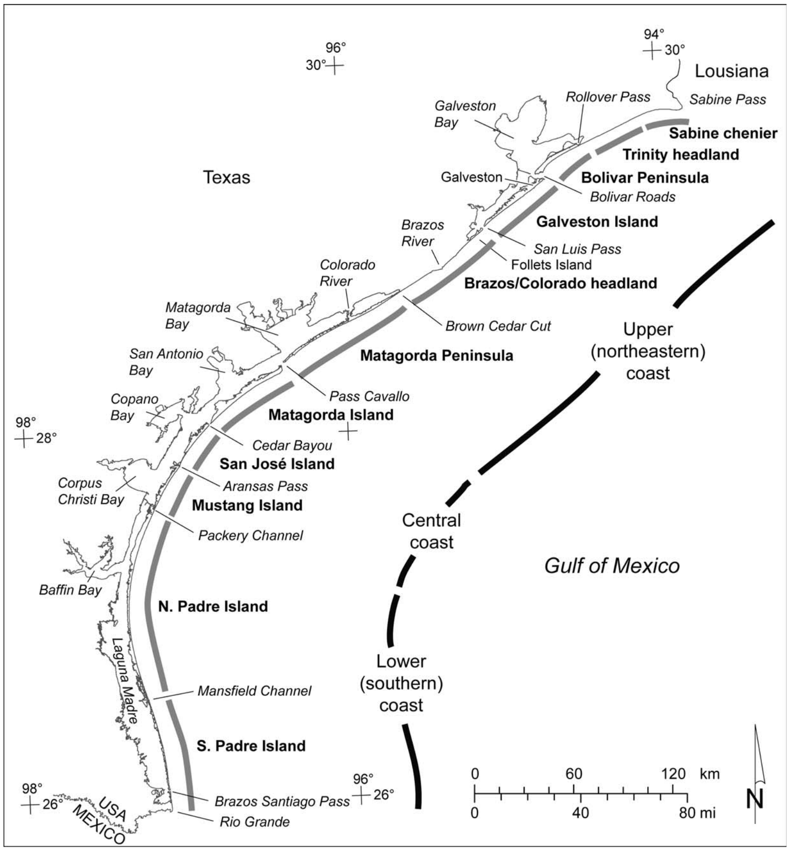

Figure 1. Map of the Texas coastal zone showing principal geomorphic features (bold). Shaded segments parallel to the shoreline indicate the approximate extent of major Holocene geomorphic features (barrier islands, peninsulas, fluvial and deltaic headlands, and strandplains).

Pass (Figure 1). Prevailing onshore, southeasterly winds generate littoral currents in the NW Gulf of Mexico that carry sediments toward a longshore convergence zone along Padre Island between the Rio Grande deltaic headland to the S and the Brazos/Colorado headland to the NE. Similarly, a smaller convergence zone occupies the embayment between the Brazos/Colorado headland and the Trinity headland along the upper Texas coast.

On the upper Texas coast, the Trinity fluvial and deltaic headland forms a mud-rich, marsh-dominated shoreline flanked by the Sabine chenier plain to the NE and Bolivar Peninsula, a sandy barrier peninsula, to the SW. Similarly, the low, mud-rich, and semiconsolidated fluvial and deltaic headland formed by the Brazos and Colorado rivers is flanked to the NE by a sandy barrier peninsula (Follets Island) and a sandy barrier island (Galveston Island) and to the SW by a sandy barrier peninsula (Matagorda Peninsula). Erosion of fluvial and deltaic headlands built by the ancestral Trinity, Brazos, and Colorado rivers contributes eroded sand to flanking sandy barriers, peninsulas, and chenier ridges and swales by longshore drift, including the Sabine chenier plain, Bolivar Peninsula, Galveston Island, Follets Island, and Matagorda Peninsula. Major coastal engineering features on the upper Texas coast that affect sediment migration and compartmentalize the coast include dredged ship channels and long jetties at Sabine Pass and Bolivar Roads, a seawall fronted by a series of rock groins on the E part of Galveston Island, and jetties protecting dredged ship channels at Freeport near the Brazos River on the Brazos/Colorado headland and at the W end of Matagorda Peninsula.

Three sandy barrier islands (Matagorda Island, San José Island, and Mustang Island) form the central Texas coast between Pass Cavallo and Packery Channel (Figure 1). These mature barrier islands have no nearby river sources of sediment but are fed by longshore currents carrying sand migrating to and from the major convergence zone along Padre Island and from the eroding Brazos/Colorado headland to the NE. A ship channel has been dredged and long jetties built at Aransas Pass, a tidal inlet separating Mustang and San José islands. The channel and protective jetties block longshore transport between Mustang and San José Island.

The lower Texas coast consists of Padre Island, a sandy and shelly barrier island that is fed by southerly and northerly longshore currents and is artificially separated into northern and southern segments at Mansfield Channel, a dredged channel protected by short jetties. A ship channel has been dredged and jetties built at Brazos Santiago Pass, which allows tidal exchange between the Gulf and Laguna Madre, a shallow lagoon landward of Padre Island. Major ship channels have been progressively deepened and widened since originally dredged and are periodically redredged to maintain specified depths.

Historical change rates of the Texas Gulf shoreline were first determined by the Bureau of Economic Geology (Bureau) in the 1970s and presented in a series of publications covering the 591 km of Gulf shoreline (Morton, 1974, 1975, 1977; Morton and Pieper, 1975a, 1975b, 1976, 1977a, 1977b; Morton, Pieper, and McGowen, 1976). This series presented net historical movement rates determined from shoreline positions drawn on 1850 to 1882 topographic charts published by the U. S. Coast and Geodetic Survey (Shalowitz, 1964) and placed at the wet-dry line mapped on aerial photographs acquired between about 1930 and 1975. Rates of change for the Texas Gulf shoreline were updated through 1982 based on aerial photographs (Morton and Paine, 1990; Paine and Morton, 1989). More recent updates for subsets of the Texas Gulf shoreline include the upper coast between Sabine Pass and the Brazos River through 1996 (Morton, 1997) and the Brazos River to Pass Cavallo (Gibeaut *et al*., 2000) and Mustang and northern Padre Island (Gibeaut *et al*., 2001) segments through 2000 using an elevation contour shoreline proxy established using an airborne LIDAR topographic mapping system. Shoreline positions in 2000–2001 were also used as part of a Gulf-wide assessment of shoreline change that included the Texas coast (Morton, Miller, and Moore, 2004). Coastwide rates of historical shoreline movement were recently updated using 2007 aerial photographs, the most recent coastwide imagery predating Hurricane Ike in 2008 (Paine, Mathew, and Caudle, 2011, 2012). These data provided the long-term context for shorter term shoreline movement that is the primary focus of this study.

Many geologic, oceanographic, meteorological, and engineering factors influence the position, movement, and status of the beach and dune system (*e.g*., McGowen, Garner, and Wilkinson, 1977). Position and movement of dynamic coastal features, particularly over a short period (three surveys over two elapsed years in this study) are affected by conditions during the time the change was measured. Beach nourishment activities, for example, can add sand to the beach system and artificially influence shoreline movement. During the study period, no major, extensive beach nourishment projects were completed. Small-scale projects are periodically completed on the Gulf shoreline along the southern and northern ends of Padre Island, on short segments of the Brazos/Colorado headland, on Galveston Island fronting the seawall and on isolated segments W of the seawall, and along the upper Texas coast on short segments of Bolivar Peninsula and the Sabine chenier plain. No major flooding events carried riverine sediments to the coast between the first airborne LIDAR survey in April 2010 and the last survey in February 2012. Two of the more significant influences on shoreline position in Texas that vary over time periods relevant to historical and shorter term aspects of this study are relative sea-level change (longer term; years to decades and longer) and tropical cyclone incidence and intensity (shorter term; hours to years).

Relative Sea Level

Changes in sea level relative to the ground surface have long been recognized as a major contributor to coastal change (*e.g*., Bruun, 1954, 1962, 1988; Cooper and Pilkey, 2004). Rising sea level inundates low-relief coastal lands causing shoreline retreat by submergence and elevates dynamic coastal processes (currents and waves) that can accelerate shoreline retreat by physical erosion. Changes in relative sea level include both changes in the ocean surface elevation ("eustatic" sea level) and changes in ground elevation caused by subsidence or uplift. Eustatic sea-level change rates, established by monitoring sea level at long-record tide gauge stations around the world and more recently using satellite altimetry, vary over a range of about 1 to 4 mm/y. Gutenberg (1941) calculated a eustatic rate of 1.1 mm/y from tide gauge data. Estimates based on tide gauge data since then have ranged from 1.0 to 1.7 mm/y (Barnett, 1983; Church and White, 2006; Gornitz and Lebedeff, 1987; Gornitz, Lebedeff, and Hansen, 1982), although Emery (1980) supported a higher global average of 3.0 mm/y that is comparable to more recent globally averaged rates based on satellite altimetry. Attempts to remove postglacial isostatic movement and geographical bias from historical tide gauge records resulted in eustatic estimates as high as 2.4 mm/y (Peltier and Tushingham, 1989). Recent studies that include satellite altimetry data acquired since 1993 indicate that the globally averaged rate of sea-level rise is 2.8 mm/y, or 3.1–3.2 mm/y with postglacial rebound removed (Cazenave and Nerem, 2004; Church *et al*., 2013; Leuliette and Willis, 2011). Much of this rise is interpreted to be caused by thermal expansion of the oceans with a possible contribution from melting of glaciers and polar ice (Cazenave and Nerem, 2004; FitzGerald *et al*., 2008; Leuliette and Miller, 2009; Leuliette and Willis, 2011).

Around the Gulf of Mexico basin, eustatic sea level rise is augmented by subsidence. Published rates of relative sea-level rise measured at tide gauges along the Texas coast are higher than eustatic sea-level rates (Lyles, Hickman, and Debaugh, 1988; Paine, 1991, 1993; Penland and Ramsey, 1990; Swanson and Thurlow, 1973). The most recent relative sea-level rise rates from selected Texas tide gauges range from 1.93 to 6.61 mm/y (Figure 2; Table 1). These rates were calculated by the National Oceanic and Atmospheric Administration through 2012 over periods of record that begin between 1908 (Galveston Pier 21) and 1963 (Port Mansfield). The highest rates (>5 mm/y) are calculated for upper and central Texas coast tide gauges at Galveston (Pier 21 and Pleasure Pier), Sabine Pass, and Rockport. The lowest rate (1.93 mm/y) is calculated for Port Mansfield on the lower (southern) coast, which also has the shortest record. The remaining gauges (Port Isabel, northern Padre Island, and Freeport) have rates between 3.48 and 4.35 mm/y.

Galveston Pier 21 has the longest period of record. The long-term rate of sea-level rise calculated from monthly averages of sea level between April 1908 and May 2014 (Figure 3) is 6.29 mm/y, similar to the NOAA-calculated rate through 2012 (Table 1). Sea-level rise at this gauge has not been constant. Calculations of average rate of change over a rolling 19-y window (chosen to match the duration of the National Tidal Datum Epoch and centered on the mid-date) show multiyear oscillations in average rate that range from 1.0 to 13.3 mm/y

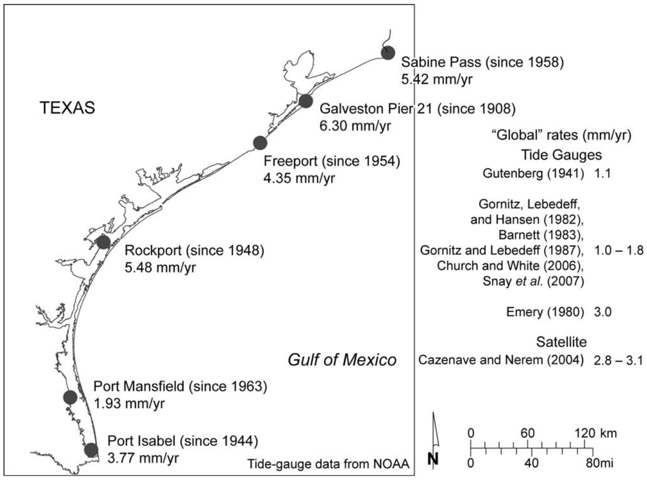

Figure 2. Relative sea-level trend at selected Texas tide gauges through 2012 and "global" rates determined from tide gauges and satellite data. Texas tide gauge data from National Oceanic and Atmospheric Administration.

(Figure 3). The most recent rates (since about 1990) are 2.2–4.9 mm/y, among the lowest observed at the gauge, and are similar to satellite altimetry–based eustatic rates for the same period. The period of the airborne LIDAR surveys (April 2010 to February 2012) coincides with relative sea-level stability as measured at Galveston Pier 21, perhaps because of reductions in subsidence related to recent shifts away from groundwater withdrawal in the Houston metropolitan area.

Tide gauge data represent single points and may not be representative of relative sea-level rise along the entire coast. Geodetic releveling data obtained from the National Geodetic Survey at benchmarks along the Texas coast from Galveston Bay to the Rio Grande show local variation in subsidence rates that would produce average rates of relative sea-level rise ranging from about 2 to more than 20 mm/y. These rates are significantly higher than both the estimated long-term subsidence rate of 0.05 mm/y or less since the last interglacial at about 100 ka (Paine, 1993) and global sea-level rise estimates but are lower than average rates of postglacial sea-level rise during the early to middle Holocene (Balsillie and Donoghue, 2004; Milliken, Anderson, and Rodriguez, 2008; Paine, Mathew, and Caudle, 2012; Shepard, 1960). Despite the wide range, most of the rates fall within the range observed for the Texas tide gauges, suggesting that the gauges are representative regional indicators of relative sea-level rise. Although these rates significantly influence shoreline change over decades and longer, they are small enough to have little to no effect on shoreline movement observed between 2010 and 2012.

Tropical Cyclones

Examples of the effect that tropical cyclones (tropical storms and hurricanes) have on Texas Gulf beach and dune systems are numerous (*e.g.*, Hayes, 1967; Morton and Paine, 1985; Price, 1956). Cyclones include tropical storms and hurricanes that are classified following the Saffir–Simpson hurricane wind scale (Simpson and Riehl, 1981). In general, minimum central

Table 1. *Long-term rates of relative sea-level rise at select Texas tide gauges (Figure 2) through 2012. Data from National Oceanic and Atmospheric Administration.*

Gauge	Beginning Year	Period (y)	Rate (mm/y)	95% Confidence Interval (mm/y)
Sabine Pass	1958	55	5.42	0.86
Galveston Pier 21	1908	105	6.35	0.26
Galveston Pleasure Pier	1957	55	6.61	0.70
Freeport (removed 2008)	1954	53	4.35	1.12
Rockport	1948	65	5.48	0.57
Port Mansfield	1963	44	1.93	0.97
Padre Island	1958	49	3.48	0.75
Port Isabel	1944	69	3.77	0.37

pressure decreases as the category increases, as does pressure- and wind-driven storm surge. Two critical parameters that increase the erosion potential of a tropical cyclone are surge height and surge duration: the longer sea level is elevated above normal during storm passage, the greater the potential for redistribution of sediment eroded from the beach. Beach and dune recovery after storm passage follows several distinct stages and can extend beyond 2 y after storm landfall (Morton and Paine, 1985; Morton, Paine, and Gibeaut, 1994).

Historical lists (Roth, 2010) and records maintained by the National Oceanic and Atmospheric Administration enumerate 64 hurricanes and 58 tropical storms that have struck the Texas coast from 1850 through 2015. On average, four hurricanes and four tropical storms make landfall in Texas per decade. From 2007 through 2012, the period most applicable to this study, seven tropical cyclones crossed the Texas coast (Table 2). This includes four tropical storms and three hurricanes that were Category 1 (Hurricane Humberto in 2007; Blake, 2007) or Category 2 (Hurricanes Dolly and Ike in 2008; Berg, 2009; Pasch and Kimberlain, 2009) at landfall. Hurricane Humberto was a short-lived, rapidly strengthening cyclone that reached Category 1 just before landfall on the Trinity headland on the upper Texas coast in September 2007. Surge heights on the upper Texas coast associated with this storm are reported at 0.6 to 1.2 m (Blake, 2007). Hurricane

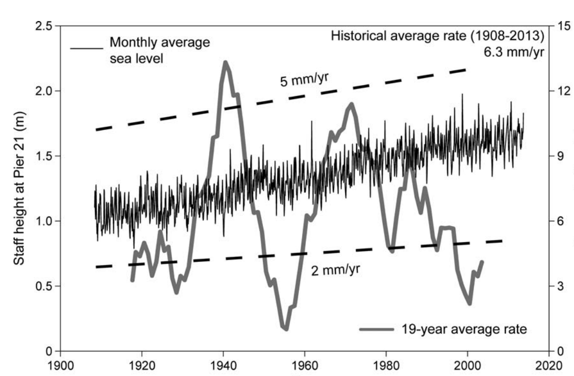

Figure 3. Sea-level trend at Galveston Pier 21, 1908–2014. Thin black line is monthly average sea level. Thick gray line is the average sea level measured over a 19-y period (the tidal datum epoch) and plotted at the center date of the period. Dashed lines indicate the slope of long-term rise at 2 and 5 mm/y. Data from National Oceanic and Atmospheric Administration.

Table 2. *Tropical cyclones affecting the Texas coast between 1990 and 2015. TD = tropical depression, TS = tropical storm, H = hurricane; number following H designates numeric strength according to the Saffir–Simpson scale (Simpson and Riehl, 1981). Only Tropical Storms Hermine (2010) and Don (2011) crossed the Texas coast between the first (2010) and last (2012) airborne LIDAR surveys considered in this study. Data from the National Oceanic and Atmospheric Administration and Roth (2010).*

Year	Category	Name	Begin Date	End Date	Landfall
1993	TS	Arlene	18 June 1993	21 June 1993	Northern Padre Island
1995	TS	Dean	28 July 1995	2 August 1995	Freeport
1998	TS	Charley	21 August 1998	24 August 1998	Aransas Pass
1998	TS	Frances	8 September 1998	13 September 1998	Matagorda Island
1999	H4	Bret	18 August 1999	25 August 1999	Padre Island (weakened)
2001	TS	Allison	5 June 2001	17 June 2001	Freeport
2002	TS	Bertha	4 August 2002	9 August 2002	Northern Padre Island
2002	TS	Fay	5 September 2002	8 September 2002	Matagorda Peninsula
2003	H1	Claudette	8 July 2003	17 July 2003	Matagorda Peninsula
2003	TS	Grace	30 August 2003	2 September 2003	Galveston Island
2005	H5	Rita	18 September 2005	26 September 2005	Sabine Pass (H3 at landfall)
2007	TS	Erin	15 August 2007	17 August 2007	San José Island
2007	H1	Humberto	12 September 2007	14 September 2007	Upper Texas coast
2008	H2	Dolly	20 July 2008	25 July 2008	Southern Padre Island
2008	TS	Edouard	3 August 2008	6 August 2008	Upper Texas coast
2008	H4	Ike	1 September 2008	15 September 2008	Galveston (H2 at landfall)
2010	TS	Hermine	5 September 2010	9 September 2010	Rio Grande area
2011	TS	Don	27 July 2011	29 July 2011	Baffin Bay area (TD at landfall)
2015	TS	Bill	15 June 2015	16 June 2015	Matagorda Island

Dolly was a Category 1 hurricane that made landfall on southern Padre Island in July 2008 accompanied by a storm surge of about 1 m (Pasch and Kimberlain, 2009). Most notable among the storms affecting shoreline position on the Texas coast within the 3-y period preceding the 2010 airborne LIDAR survey is Hurricane Ike, once a Category 4 storm that weakened before landfall, yet severely eroded central and upper Texas coast beaches as a very large Category 2 storm associated with an unusually high and long-duration storm surge in September 2008 (Berg, 2009). Ike caused elevated water levels along the entire U.S. Gulf of Mexico coast; open-coast surge heights reached 4–5 m on the upper Texas coast, more than 3 m on the Brazos/Colorado headland, and 1–2 m on the lower coast (Berg, 2009).

The initial airborne LIDAR survey for this study occurred in April 2010, which allowed 1.5–2.5 y of beach and dune recovery after Hurricanes Ike, Humberto, and Dolly. During the 2010 to 2012 airborne LIDAR survey period, only Tropical Storm Hermine (September 2010) and Tropical Storm Don (July 2011) affected the Texas coast. Hermine made landfall on the NE coast of Mexico on 7 September 2010 accompanied by winds of 110 km/h and surge heights of 0.5–1.0 m along the southern Texas coast (Avila, 2010). Don weakened to a tropical depression as it made landfall on Padre Island just N of Baffin Bay on 30 July 2011 (Brennan, 2011). The maximum recorded surge height was 0.6 m on northern Padre Island (Brennan, 2011). Neither of these tropical storms had a strong effect on Texas Gulf shoreline position or beach and dune morphology.

METHODS

Annual airborne LIDAR surveys conducted by the Bureau in April 2010, April 2011, and February 2012 covered a swath about 500-m wide along the entire Texas Gulf shoreline that included the beach and adjacent major dune systems. LIDAR and associated GPS data were processed to produce point clouds and 1-m-resolution digital elevation models (DEMs) of the ground surface. Shoreline position for each annual LIDAR survey was determined by extracting a common elevation contour as the shoreline proxy. Shoreline movement between each annual survey and for the entire monitoring period (2010–2012) was determined and compared with historical shoreline change rates determined through 2007. DEMs were also used to examine relationships among the principal geomorphic coastal segments (Figure 1) in surface area above threshold elevations at 1-m elevation intervals. Differences in areas above threshold elevations calculated for geomorphic features on the coast can reveal significant differences in subaerial sand storage, erosion resilience, and storm flooding susceptibility.

Principal tasks included (1) planning, acquiring, and processing the airborne LIDAR data for three annual surveys of the Texas Gulf shoreline; (2) producing full-resolution point clouds and DEMs; (3) extracting a shoreline proxy from the DEMs to analyze short-term shoreline change; and (4) analyzing DEMs to assess subaerial sand storage, storm surge susceptibility, and erosion resilience.

LIDAR Data Acquisition

Three annual airborne LIDAR surveys were completed for the Texas Gulf shoreline from Sabine Pass to the Rio Grande in 2010, 2011, and 2012 (Paine, Caudle, and Andrews, 2013). The LIDAR system (Optech Inc. ALTM 1225) was installed in a single-engine Cessna 206 aircraft. LIDAR instrument settings for these flights were 25 kHz laser pulse rate, 26 Hz laser scanner rate, ±20 degrees scan angle, 570–1200 m flight altitude (depending on cloud altitude), and 36–62 m/s ground speed. The survey swath was approximately 500 m wide, covering the beach and dune system.

The 2010 survey was flown over 5 d between 8 and 24 April, the 2011 survey was flown over 6 d between 6 and 16 April, and the 2012 survey was flown over 6 d between 14 and 26 February (Paine, Caudle, and Andrews, 2013). Twelve GPS base station locations were occupied during the LIDAR surveys to improve final flight trajectories. The base stations were distributed along the coast on the Trinity headland, Bolivar Peninsula, Galveston Island, Brazos/Colorado headland, Matagorda Peninsula, on San Antonio Bay near Matagorda Island, Mustang Island, and northern and southern Padre Island. Additional ground GPS control was provided by continuously operating reference stations at three sites on the upper and central Texas coast.

LIDAR Data Processing

Base station coordinates were computed using the National Geodetic Survey's Online Positioning User Service software. Aircraft trajectories for each base station were computed using the National Geodetic Survey's KINPOS software. Trajectories determined from each base station were merged for each flight. Weighting for the trajectory merge is based on baseline length (distance from base station) and solution root mean square errors. The trajectory solution was transformed from the International Terrestrial Reference Frame of 2000 to the North American Datum of 1983 (NAD83) using the National Geodetic Survey's horizontal time-dependent positioning software. The NAD83 trajectories and aircraft inertial measurement unit data were input into Applanix's POSProc version 2.1.4 to compute an optimal 50-Hz inertial navigation solution (INS) and smoothed best estimate of trajectory (SBET). The new INS and SBET were substituted into Realm 2.27 software to generate a set of initial LIDAR instrument calibration parameters (pitch, roll, and scale) for each flight. The parameters were incrementally improved by iteratively comparing a subset of the LIDAR output to GPS kinematic ground control.

Ground GPS surveys were conducted for calibration and ground truth elevations. The ground survey points are estimated to have a vertical accuracy of 0.01–0.05 m. Roads and open areas with an unambiguous surface were surveyed using a kinematic GPS method. A LIDAR data set was sorted to gather data points within 0.5 m of a ground GPS survey point. The mean difference between the LIDAR- and ground GPS–derived elevations was used to estimate and remove elevation bias from the LIDAR data, which ranged from –0.18 to +0.07 m for the 2010 survey, –0.21 to +0.22 m for the 2011 survey, and –0.15 to +0.23 m for the 2012 survey. The standard deviation of the ground GPS– and LIDAR-derived elevation differences provide an estimate of LIDAR precision; these range from 0.04 to 0.10 m for the 2010 survey, 0.03 to 0.13 m for the 2011 survey, and 0.08 to 0.23 m for the 2012 survey. The bias-corrected LIDAR returns were gridded to create DEMs using a weighted inverse distance algorithm to determine cell values. The Geiod99 model was applied to the grids to convert z values from height above the GRS80 ellipsoid to elevations with respect to the North American Vertical Datum 88 (NAVD88). Tide gauge data from Texas coastal stations show that elevations relative to the NAVD88 datum can differ from local mean sea level by values that vary along the coast from 0.15 m below msl on the upper coast at Galveston to 0.01 m above msl on the lower coast near southern Padre Island (U. S. Department of Commerce, National Oceanic and Atmospheric Administration, unpublished data).

Shoreline Position

Before the advent of airborne LIDAR, vertical aerial photographs were commonly used to determine shoreline position. Shorelines were drawn on, or digitized from, the photographic images, generally at the distinct tonal boundary between wet and dry sand on the beach. The position of this boundary can vary over several meters because of water level, wave activity, and georeferencing errors. Through analysis of LIDAR surveys and beach profiles, Gibeaut and Caudle (2009) and Gibeaut, Gutierrez, and Hepner (2002) determined that the wet-dry boundary occurs at about 0.6 m above msl on the Texas Gulf shoreline. Because mean sea level is a local datum that varies spatially and temporally, DEMs constructed from LIDAR data are referenced to the fixed NAVD88 datum. Using the most seaward, continuous contour of 0.6 m NAVD88 from the LIDAR-derived DEM provides a consistent shoreline feature among LIDAR data sets when water level and wave activity may differ but will differ from mean sea level along the Texas coast according to the local difference between mean sea level and NAVD88. That difference is negligible for the southern Texas coast but reaches about 0.15 m at Galveston on the upper Texas coast. Given the average beach slope on the Texas coast of about 0.04 m/m determined from beach profiles acquired during this study, the elevation difference translates to a potential lateral shift of less than 4 m that is consistent among the 2010, 2011, and 2012 LIDAR surveys. Errors in LIDAR-derived elevation, estimated to be about 0.1 m or less on the basis of comparisons with ground GPS measurements, translates to a potential lateral shoreline position error of 2–3 m.

To extract a consistent shoreline proxy from the airborne LIDAR data, the 2010, 2011, and 2012 DEMs were imported into an ESRI ArcMap geographic information system, and the 0.6-m NAVD88 contour was determined. The extracted contour was edited in ArcMap to retain the most seaward, continuous contour and smoothed using a 2-m smoothing tolerance. Shoreline movement between each pair of shorelines (2010–2011, 2011–2012, and 2010–2012) was measured along 11,783–11,811 shore-normal transects spaced at 50-m intervals along the Texas Gulf shoreline using the Digital Shoreline Analysis System within ArcGIS (Thieler *et al.*, 2009). The number of transects varied slightly among the comparison years owing to lateral migration of passes and channels. The same transects were used for each shoreline comparison.

Elevation Threshold Areas

Extracting an elevation contour from the DEM and using it as a proxy for shoreline position is a convenient way to examine shoreline position and movement over time, but much more information is available from a DEM that covers the beach and dune system. In particular, the DEM can be "sliced" at arbitrary elevations, readily yielding the area that is at or above that elevation. Beginning with the 2-m elevation threshold, which is the lowest elevation that (1) exceeds common wet and dry beach elevations seaward of the dunes and the vegetated barrier flats and marshes landward of the dunes and (2) includes elevations typical of incipient and mature dunes, the total number of DEM grid cells that exceeds the chosen elevation was calculated for each LIDAR survey and each major geomorphic feature. The threshold, or minimum, elevation was then increased at 1-m increments to a maximum elevation of 9 m, and the total number of DEM cells exceeding each threshold elevation was calculated. Plotting threshold elevation against grid cell area exceeding that elevation for each segment of the Texas Gulf shoreline produces elevation threshold area, or ETA, relationships that reveal several important attributes related to coastal landform morphology. These include (1) susceptibility to storm surge and flooding at arbitrary surge heights, (2) sand storage within the beach and dune system, (3) maturity and extent of dunes, and (4) resistance to, and recoverability from, chronic and instantaneous erosion events. ETA curves also provide a rapid framework in which to monitor area and volume change over time, which enables a more complete understanding of beach and dune system behavior.

RESULTS

Short-term shoreline movement determined from the three annual airborne LIDAR surveys in 2010, 2011, and 2012 was analyzed in the context of historical shoreline movement rates updated through 2007 (Paine, Mathew, and Caudle, 2011, 2012). These historical rates have recently been updated again through 2012 (Paine, Caudle, and Andrews, 2014). The rates through 2007 are used in this study to separate the influence of Hurricane Ike (2008), the most impactful of recent storms to strike the Texas coast, from the historical trends and to ensure that the types of shoreline proxies used are consistent within each data set. For the historical trends, shoreline rates are based largely on positions determined from aerial photographs. For the short-term (2010–2012) study, shoreline movement is based on the changing position of the 0.6-m NAVD88 elevation contour used as the shoreline proxy.

Historical Texas Gulf Shoreline Movement

Historical rates of Gulf shoreline movement, calculated from multiple shoreline positions between the 1930s (mid to late 1800s in some areas) and 2007 (Paine, Mathew, and Caudle, 2012), average 1.3 m/y of retreat (Figure 4) for both net (or endpoint) rate (net movement rate between the oldest shoreline position and the 2007 position) and linear regression rate (best-fit movement rate for all shoreline positions in a least-squares sense) calculations. Historical rates were calculated at 11,731 sites spaced at 50-m intervals along the entire Texas coast. Net retreat occurred at 9830 sites (84%) and advance occurred at 1880 sites (16%). Shorelines along the upper Texas coast (from Sabine Pass to the Colorado River) generally retreated at greater rates than those on the central and lower coast. Averages of movement rates were retreat at 1.6 m/y for the upper coast and retreat at 1.0 m/y for the central and lower coast.

Notable extensive areas of relatively high long-term retreat rates ($\geq$1.5 m/y) include (1) the Trinity fluvial and deltaic headland and Sabine chenier plain on the upper Texas coast; (2) a segment W of the seawall on Galveston Island, a sandy barrier island on the upper Texas coast; (3) the fluvial and deltaic headland of the Brazos and Colorado rivers; (4) Matagorda Peninsula, a sandy barrier peninsula W of the Colorado River; (5) San José Island, a sandy central Texas coast barrier island; (6) the northern part and most of the southern half of Padre Island, a sandy barrier island on the lower Texas coast; and (7) near the mouth of the Rio Grande S of Brazos Santiago Pass (Figure 4). Areas of general net shoreline advance are found (1) on the upper coast near jetties at Sabine Pass and Bolivar Roads, (2) at the W tip of Galveston Island, (3) near the mouth of the Brazos River, (4) on the W end of Matagorda Peninsula, (5) on the central Texas coast along much of Matagorda Island and near Aransas Pass, and (6) on Padre Island near Baffin Bay and the southern end of the island. The average annual rate of land loss along the Texas Gulf shoreline is 74 ha/y. Total Texas Gulf shoreline land loss from 1930 through 2007 is estimated to be 5670 ha.

Presurvey Shoreline Movement between 2007 and 2010

Passage of Hurricanes Humberto (2007), Dolly (2008), and Ike (2008) across the Texas coast (Table 2) occurred after the historical shoreline movement study period ended in 2007 and before the first airborne LIDAR survey of the Texas Gulf shoreline was completed in 2010. To evaluate the shoreline movement associated with the sudden erosion and gradual recovery from these storms, the shoreline position extracted from the April 2010 airborne LIDAR survey DEM at the 0.6-m NAVD88 elevation contour was compared with the September–October 2007 shoreline position determined using the wet-dry line as mapped on aerial photographs. Because annualized rates of change can be misleading over such short time periods, short-term movement is presented as distances rather than rates.

Over the 2.5-y period between the 2007 and 2010 shorelines, the Texas Gulf shoreline retreated at about 73% and advanced at about 27% of 11,785 monitoring sites. The shoreline moved an average of 7.1 m landward, resulting in a net land loss of 417 ha. Over the short comparison period, this movement translates to average rates of retreat (2.8 m/y) and land loss (167 ha/y) that are greater than historical averages (1.3 m/y and 74 ha/y; Figure 4). Greatest average amounts of retreat were documented on geomorphic features most affected by the 2007 and 2008 storms, including the Trinity headland and Sabine chenier plain (23 m), Galveston Island (6 m), and the Brazos/Colorado headland (5 m) on the upper Texas coast; Matagorda Island (10 m) on the central Texas coast; and northern (6 m) and southern (10 m) Padre Island on the lower Texas coast. Given the potentially severe impact and extended recovery period observed for storms affecting the Texas coast (*e.g.*, Morton and Paine, 1985; Morton, Paine, and Gibeaut, 1994), recovery from these storms likely continued into the 2010–2012 period covered by the annual airborne LIDAR surveys.

Short-Term Shoreline Movement 2010–2012

Short-term shoreline change was determined for the three annual airborne LIDAR surveys by (1) extracting the 0.6-m NAVD88 elevation contour from each data set and using that as the shoreline proxy and (2) calculating distances between each shoreline (2010–2011, 2011–2012, and 2010–2012) at about 11,800 measurement locations spaced at 50-m intervals along the Texas Gulf shoreline.

Incremental Movement between 2010 and 2011

The Texas Gulf shoreline predominantly advanced between April 2010 and April 2011 (Figure 5). Change measured along

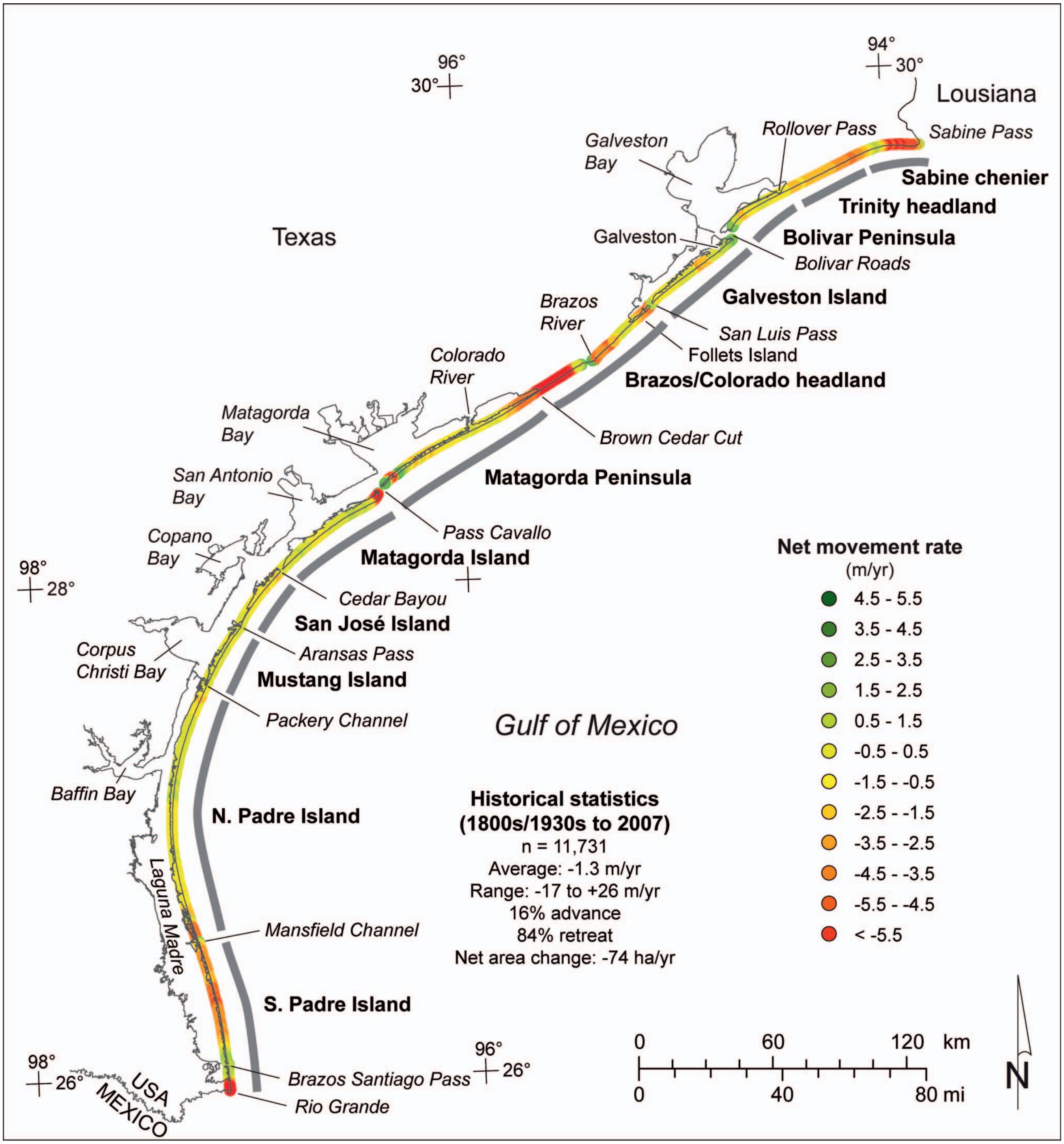

Figure 4. Net rates of long-term change along the Texas Gulf shoreline calculated from the earliest reliable shoreline position (late 1800s or 1930s) through 2007 (updated from Paine, Mathew, and Caudle, 2011, 2012). Rates of change were calculated at 11,731 measurement sites spaced at 50-m intervals along the Gulf shoreline.

the coast was positive (advancing) at 75% of the 11,783 measurement sites; the average distance of shoreline advance was 6.5 m. There was a net gain in beach area during this period of 382 ha.

Varying amounts of shoreline movement were measured along the coast (Figure 5; Table 3). Galveston Island shoreline advanced the most (12.2 m average), with notable areas of advance adjacent to the S jetty at Bolivar Roads and along

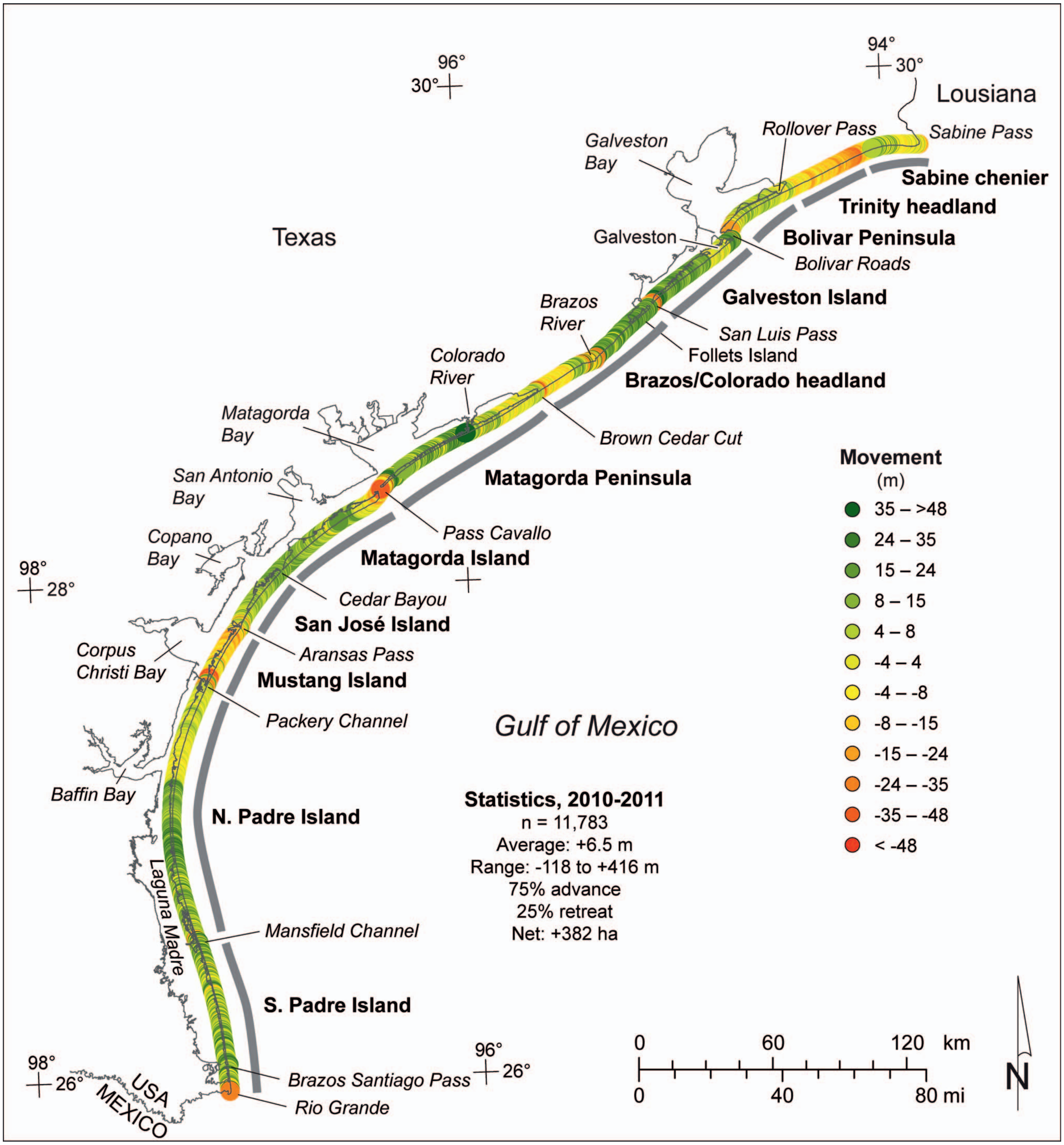

Figure 5. Net shoreline change along the Texas Gulf shoreline between April 2010 and April 2011. Change calculated from shoreline positions determined from airborne LIDAR surveys. Positive values indicate shoreline advance; negative values indicate shoreline retreat. Rates of change were calculated at 11,783 measurement sites spaced at 50-m intervals along the Gulf shoreline.

much of the W part of the island, except near San Luis Pass. Bolivar Peninsula shoreline also advanced an average of 4.5 m (Table 3), with only the segment near the N jetty at Bolivar Roads retreating (Figure 5). An average advance of between 5 and 10 m was measured along the Brazos/Colorado headland (including Follets Island), Matagorda Peninsula, Matagorda Island, San José Island, and northern and southern Padre Island.

Table 3. *Net shoreline change determined from shoreline position extracted from airborne LIDAR data acquired in April 2010 and April 2011. Locations shown on Figure 5.*

Area	No.	Net Change (m)	SD (m)	Range (m)	Land Area Change (ha)
All Texas sites	11,783	6.5	12.3	−118 to 416	+382.1
Coastal sections					
Upper coast (Sabine Pass to Bolivar Roads)	1894	−0.9	8.2	−110 to 40	−8.7
Upper central coast (Bolivar Roads to Pass Cavallo)	3777	9.4	15.0	−118 to 416	+177.0
Lower central coast (Pass Cavallo to Packery Channel)	2329	4.4	9.5	−81 to 55	51.5
Lower coast (Packery Channel to Rio Grande)	3755	8.7	10.5	−82 to 175	+162.9
Geomorphic features					
Sabine chenier and Trinity headland	1337	−3.2	7.6	−29 to 40	−21.2
Bolivar Peninsula	557	4.5	7.1	−110 to 31	+12.5
Galveston Island	937	12.2	20.7	−118 to 416	+57.0
Brazos/Colorado headland	1252	8.3	13.2	−58 to 124	+52.2
Matagorda Peninsula	1582	8.7	11.3	−49 to 84	+68.8
Matagorda Island	1152	6.9	7.1	−19 to 55	+39.5
San José Island	627	8.9	5.0	−10 to 25	+27.8
Mustang Island	575	−5.7	10.1	−81 to 19	−16.4
Northern Padre Island	2399	8.0	11.4	−82 to 175	+96.5
Southern Padre Island	1356	9.8	8.8	−44 to 44	+66.4

Only two major coastal shoreline segments underwent average shoreline retreat between 2010 and 2011. These included the Trinity headland and Sabine chenier plain on the upper Texas coast (average retreat of 3.2 m; Table 3), along the historically erosional stretch of low marsh, and Mustang Island (average retreat of 5.7 m), along the historically relatively stable to minimally erosional central Texas coast (historical retreat rates of $\leq$1 m/y; Figure 4).

Incremental Movement between 2011 and 2012

Between the April 2011 and February 2012 airborne surveys, Texas Gulf shorelines predominantly returned to the historical recessional trend (Figures 4 and 6). Shoreline movement measured at 11,811 sites along the coast averaged 3.1 m of retreat; the shoreline retreated at 67% of measurement sites, with a net loss of 181 ha of beach area between April 2011 and February 2012.

With the exception of the barrier islands on the central Texas coast, shorelines retreated along all major geomorphic features. The greatest amount of retreat occurred on Padre Island, where average retreat was 7.2 m on northern Padre Island and 8.9 m on southern Padre Island (Figure 6; Table 4). Amounts of retreat also generally increased northward from the central to NE part of the coast, where an average retreat of 3.3 m on Matagorda Peninsula increased to 5.7 m on the Trinity headland and Sabine chenier plain. Average retreat on Galveston Island was 2.7 m, slightly less than adjacent segments to the NE and SW of the island. Central coast barrier island shorelines advanced average distances that increased southward: 5.2 m on Matagorda Island, 5.9 m on San José Island, and 11.7 m on Mustang Island.

Net Change between 2010 and 2012

Predominant retreat along 67% of the Texas Gulf shoreline between 2011 and 2012 did not fully offset advance along 75% of the shoreline between 2010 and 2011. Consequently, shoreline position in February 2012 remained seaward of its position in April 2010 at 59% of the 11,811 measurement sites along the coast (Figure 7). The average movement was 3.4 m seaward (Figure 7; Table 5), resulting in a net gain in beach area of 203 ha between 2010 and 2012.

Shorelines along the central coast (Matagorda Island and San José Island) and Galveston Island advanced on average about 10–15 m (Figure 7; Table 5). Shorelines to the NE and SW of the advancing central coast also advanced, but over smaller distances (about 5 m along Matagorda Peninsula and the Brazos/Colorado headland to the NE and Mustang Island to the SW). Small amounts of average advance or retreat ($\leq$1 m) were measured along Bolivar Peninsula and Padre Island that are within the possible lateral error associated with the shoreline position extracted from LIDAR-derived DEMs. Significant average retreat was measured only along the upper Texas coast along the Trinity headland and Sabine chenier plain (9 m; Table 5), the only major geomorphic features on the Texas coast where average retreat was measured for both 2010–2011 and 2011–2012 (Figure 7). Conversely, the most significant shoreline advance for 2010–2012 was measured along two central Texas coast barrier islands (Matagorda Island and San José Island), which were the only major geomorphic features where average shoreline advance was measured in both periods (2010–2011 and 2011–2012).

ETAs on the Texas Coast 2010–2012

Total areas above threshold elevations were determined for the April 2010, April 2011, and February 2012 airborne surveys to produce annual composite ETA curves for the entire Texas Gulf shoreline (Figure 8). These curves, determined over a 300- to 500-m-wide swath along the Gulf shoreline, reveal a sharp reduction in total area as threshold elevations increase. At 2-m elevation, for example, which is the approximate elevation that separates the beach environments from the dune environments (Figure 8), the coastal swath encompasses 66 (in 2011) to 77 (in 2012) km^2 of area at or above that elevation. Above the 3-m threshold, less than half that area (31–34 km^2, depending on the year) is at or above that elevation. The reduction in surface area by approximately half with each 1-m increase in threshold elevation holds throughout the elevation range. At the highest threshold elevation of 9 m, less than 1 km^2 of area within the LIDAR swath exceeds that elevation.

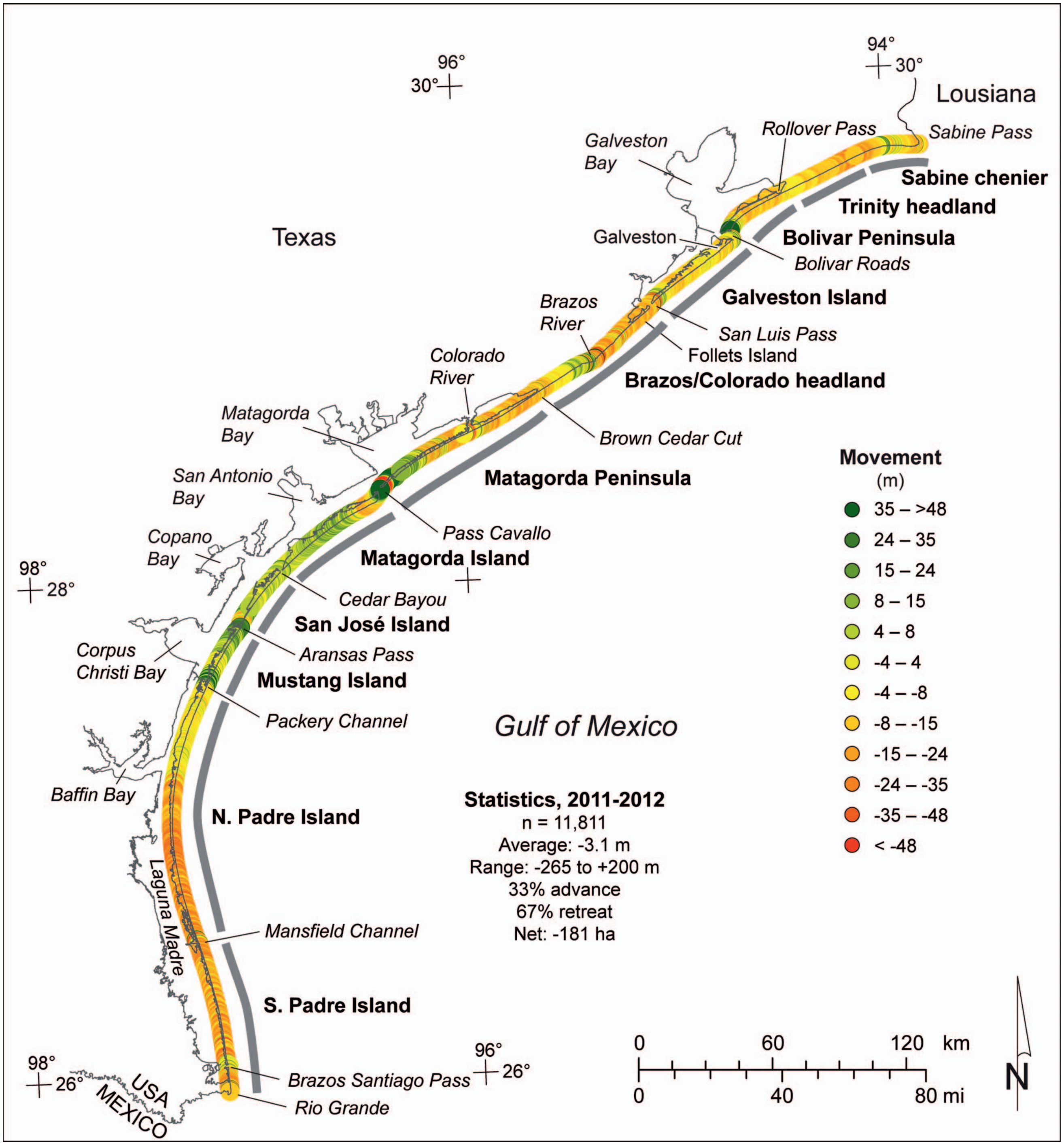

Figure 6. Net shoreline change along the Texas Gulf shoreline between April 2011 and February 2012. Change calculated from shoreline positions determined from airborne LIDAR surveys. Positive values indicate shoreline advance; negative values indicate shoreline retreat. Rates of change were calculated at 11,811 measurement sites spaced at 50-m intervals along the Gulf shoreline.

ETA curves can be constructed for any surveyed area or location. To illustrate some of the differences in morphology evident along the Texas Gulf shoreline, ETAs were calculated for upper, central, and lower coast features (Figure 9) using 2012 airborne survey data. To standardize the comparison among geomorphic features with differing shoreline lengths, the ETA curves have been normalized by dividing the threshold areas by the shoreline length along each feature. In this form,

Table 4. *Net shoreline change determined from shoreline position extracted from airborne LIDAR data acquired in April 2011 and February 2012. Locations shown in Figure 6.*

Area	No.	Net Change (m)	SD (m)	Range (m)	Land Area Change (ha)
All Texas sites	11,811	−3.1	14.3	−265 to 200	−180.5
Coastal sections					
Upper coast (Sabine Pass to Bolivar Roads)	1899	−5.5	7.3	−123 to 58	−52.1
Upper central coast (Bolivar Roads to Pass Cavallo)	3798	−3.4	18.6	−265 to 200	−63.8
Lower central coast (Pass Cavallo to Packery Channel)	2329	6.9	9.0	−16 to 121	+80.3
Lower coast (Packery Channel to Rio Grande)	3757	−7.8	11.3	−173 to 109	−166.6
Geomorphic features					
Sabine chenier and Trinity headland	1342	−5.7	6.4	−41 to 30	−38.0
Bolivar Peninsula	557	−5.1	9.0	−123 to 58	−14.2
Galveston Island	938	−2.7	14.0	−151 to 140	−12.9
Brazos/Colorado headland	1257	−4.2	14.2	−123 to 200	−26.2
Matagorda Peninsula	1596	−3.3	23.1	−265 to 79	−26.5
Matagorda Island	1152	5.2	7.2	−15 to 31	+29.7
San José Island	627	5.9	6.2	−16 to 26	+18.4
Mustang Island	575	11.7	12.3	−9 to 121	+33.6
Northern Padre Island	2399	−7.2	12.7	−174 to 109	−86.0
Southern Padre Island	1358	−8.9	8.3	−48 to 25	−60.7

they become a generalized beach profile showing average beach and dune system widths for the feature at each elevation threshold (conceptually, ETA values cast as an area per unit length of shoreline can be converted to a distance that represents average shore-normal width above a given threshold elevation).

Upper Coast

Upper coast ETA curves (Figure 9a) include those for the Sabine chenier plain and the Trinity headland, Bolivar Peninsula and Galveston Island, the NE part of the Brazos/Colorado headland, and the SW part of the Brazos/Colorado headland and Matagorda Peninsula, extending from Sabine Pass to Pass Cavallo (Figure 1). Shorelines on the Trinity headland and Sabine chenier plain are the most rapidly retreating in Texas. The ETA curve for this area has the smallest normalized area (or average shore-normal width) above any threshold elevation for any geomorphic area, along with the lowest elevation above which virtually no area exists within the LIDAR survey swath (4 m; Figure 9a). At Sea Rim State Park on the Sabine chenier plain (Figure 10), for example, the LIDAR-derived DEM along the shoreline (Figure 10b) shows numerous shore-normal erosional features and generally low elevation (mostly <3 m). Area slices at threshold elevations of 2 m (Figure 10c) and 3 m (Figure 10d) show how little of the land surface exceeds those relatively low elevations. The ETA curve readily reveals that this area is highly susceptible to widespread flooding at low to moderate surge heights of 2 m or less, that sand storage in the beach and dune system is minimal, and that the area is highly susceptible to chronic erosion.

ETA curves for Bolivar Peninsula, Galveston Island, Follets Island, and the NE part of the Brazos/Colorado headland each show considerably more normalized area above each threshold elevation (Figure 9a). Maximum threshold elevation for these features is about 8 m, above which little area remains. About twice as much normalized area is above a given threshold elevation on Bolivar Peninsula and Galveston Island as on Follets Island and the Brazos/Colorado headland, but a significant fraction of the area at higher threshold elevations is artificially elevated along and landward of the seawall at Galveston. The SW part of the Brazos/Colorado headland and Matagorda Peninsula have the second lowest maximum elevation threshold at about 5 m (just above the maximum for the Sabine chenier plain and Trinity headland) and also have the second lowest normalized area (or average shore-normal width) at threshold elevations above 3 m of the upper coastal segments (Figure 9a).

Central Coast

Central coast ETA curves include Matagorda Island, San José Island, and Mustang Island. These areas are within the least erosional part of the Texas coast, where average rates of historical shoreline retreat range from 0.4 to 1.1 m/y (Figure 4). ETA curves for these geomorphic features are progressively higher and wider from N to S, following the trend of southward-decreasing retreat rates. Matagorda Island has a similar curve to that of Matagorda Peninsula to the NE but has slightly greater normalized area at threshold elevations of 2 and 3 m. A DEM and series of elevation slices at a site on Matagorda Island (Figure 11) demonstrate the difference in morphology between a more stable central coast setting and the highly erosional upper coast site at Sea Rim State Park (Figure 10). The DEM on Matagorda Island shows prominent ridge-and-swale features that reach maximum elevations above 5 m (Figure 11b). Slices through the DEM at 2, 3, 4, and 5 m (Figures 11c–f) show large normalized areas exceeding lower threshold elevations, along with progressively more limited areas exceeding higher threshold areas farther onshore on the mature dune crests.

Farther S along the central coast, San José Island has a significantly higher maximum threshold elevation of about 8 m than areas farther to the NE (Figure 9b). It also has normalized areas (or average shore-normal widths) above threshold elevations of 2–6 m that considerably exceed those for the Brazos/Colorado headland, Matagorda Peninsula, and Matagorda Island. The most robust ETA curves are found farther to the SW on Mustang Island, where normalized areas above threshold elevations are the highest of any along the central Texas coast (Figure 9b).

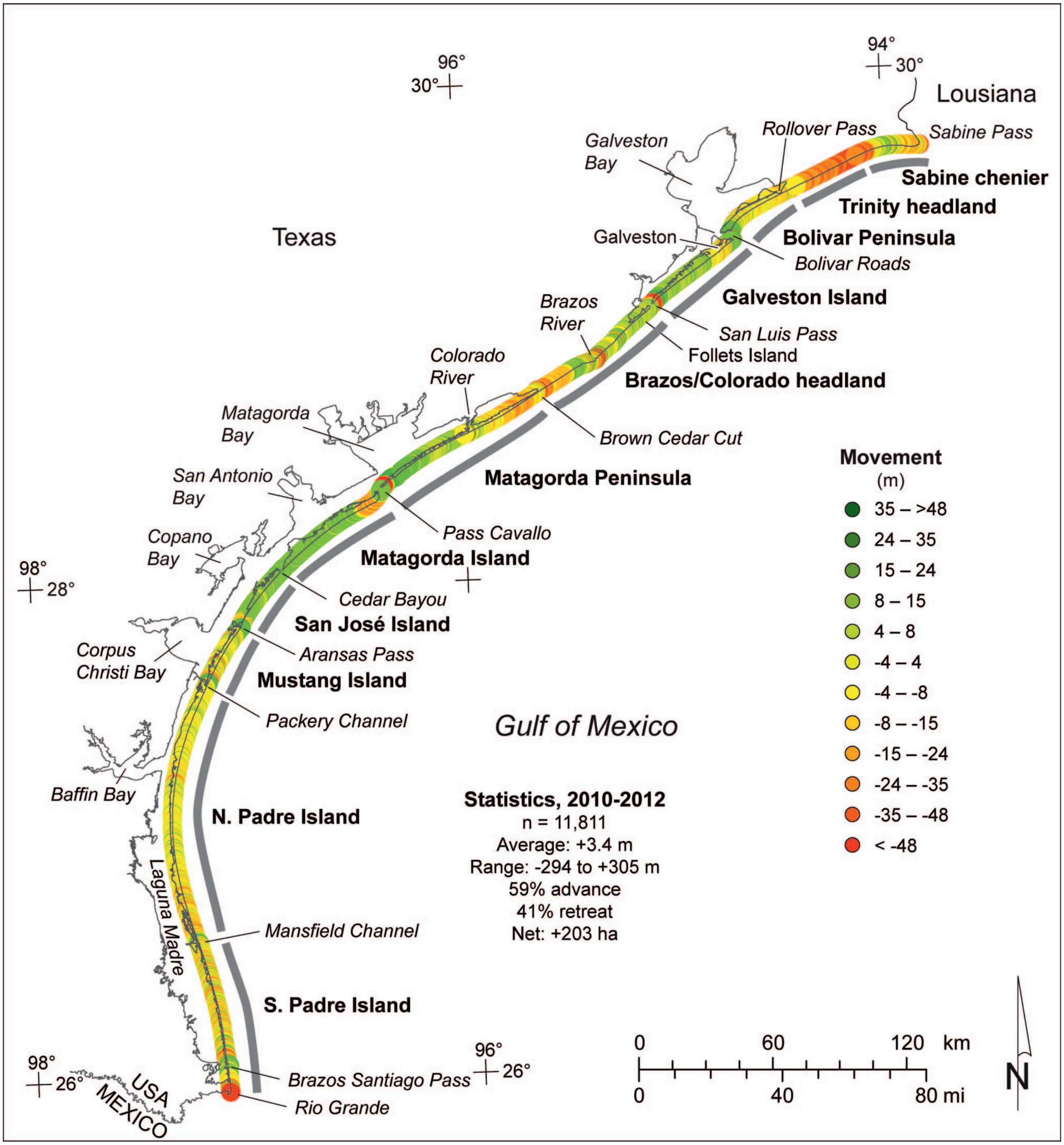

Figure 7. Net shoreline change along the Texas Gulf shoreline between April 2010 and February 2012. Change calculated from shoreline positions determined from airborne LIDAR surveys. Positive values indicate shoreline advance; negative values indicate shoreline retreat. Rates of change were calculated at 11,811 measurement sites spaced at 50-m intervals along the Gulf shoreline.

Lower Coast

The lower coast ETA curves were distributed among four sections on the northern, central, and southern parts of Padre Island (Figure 9c). Average rates of historical shoreline retreat generally increase southward along Padre Island, increasing from 0.8 m/y on northern Padre Island to 2.3 m/y on southern Padre Island (Figure 4). ETA curves for Padre Island have relatively high maximum threshold elevations of 9 m or more

Table 5. *Net shoreline change determined from shoreline position extracted from airborne LIDAR data acquired in April 2010 and February 2012. Locations shown in Figure 7.*

Area	No.	Net Change (m)	SD (m)	Range (m)	Land Area Change (ha)
All Texas sites	11,811	3.43	16.0	−294 to 305	+202.6
Coastal sections					
Upper coast (Sabine Pass to Bolivar Roads)	1899	−6.38	11.8	−138 to 40	−60.6
Upper central coast (Bolivar Roads to Pass Cavallo)	3798	5.99	22.2	−294 to 305	+113.8
Lower central coast (Pass Cavallo to Packery Channel)	2329	11.3	10.8	−34 to 61	+131.8
Lower coast (Packery Channel to Rio Grande)	3757	0.9	8.0	−25 to 73	+16.5
Geomorphic features					
Sabine chenier and Trinity headland	1342	−8.8	11.6	−44 to 40	−59.0
Bolivar Peninsula	557	−0.6	10.1	−138 to 26	−1.6
Galveston Island	938	9.4	19.2	−124 to 305	+44.1
Brazos/Colorado headland	1257	4.1	17.8	−151 to 233	+26.0
Matagorda Peninsula	1596	5.3	26.4	−294 to 84	+42.5
Matagorda Island	1152	12.0	10.5	−17 to 61	+69.2
San José Island	627	14.7	7.3	−10 to 32	+46.2
Mustang Island	575	6.0	12.4	−34 to 41	+17.2
Northern Padre Island	2399	0.9	7.1	−20 to 73	+10.5
Southern Padre Island	1358	0.9	9.4	−25 to 36	+6.0

(Figure 9c), but those in the southernmost section of the island are skewed at the higher elevations by the presence of structures within the LIDAR swath. Near the convention center on southern Padre Island, for example, the LIDAR-derived DEM has a maximum elevation exceeding 10 m (Figure 12b), showing the presence of high, mature dunes as well as rectangular buildings. Elevation slices through the DEM at 2, 4, 6, and 8 m (Figures 12c–f) show progressively decreasing areas exceeding those elevations. At the highest elevation shown (8 m), only the crest of a high, mature dune and nearby buildings remain.

ETA curves for the southern part of Padre Island are similar to those for the northern part of Padre Island at the higher elevation thresholds (6 m and higher), but have significantly

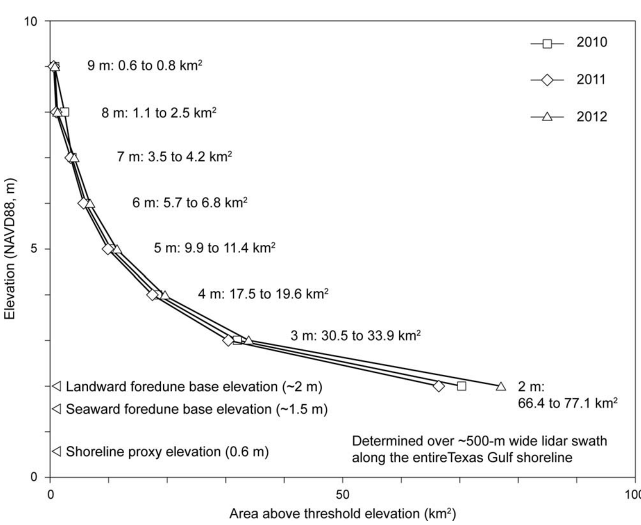

Figure 8. Total area above threshold elevations in 2010, 2011, and 2012 in a swath covering the beach and dune system along the entire Texas Gulf shoreline. Areas were calculated by aggregating DEM grid cell counts above threshold elevations.

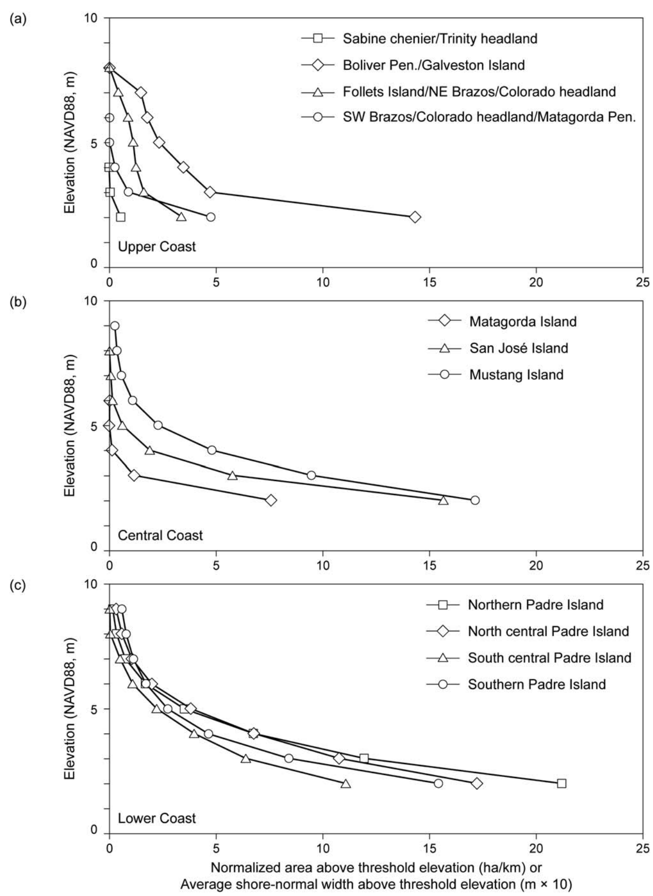

Figure 9. Normalized area above threshold elevations for geomorphic features of upper, central, and lower Texas Gulf shoreline. Multiplying the *x* axis values by 10 yields a generalized beach profile showing average shore-normal widths (m) above threshold elevations. ETA curves calculated from 2012 LIDAR-derived DEMs. Areas (DEM 1-m grid cell counts) are normalized by dividing the total area above a given threshold elevation in the geomorphic feature by the alongshore extent of the feature.

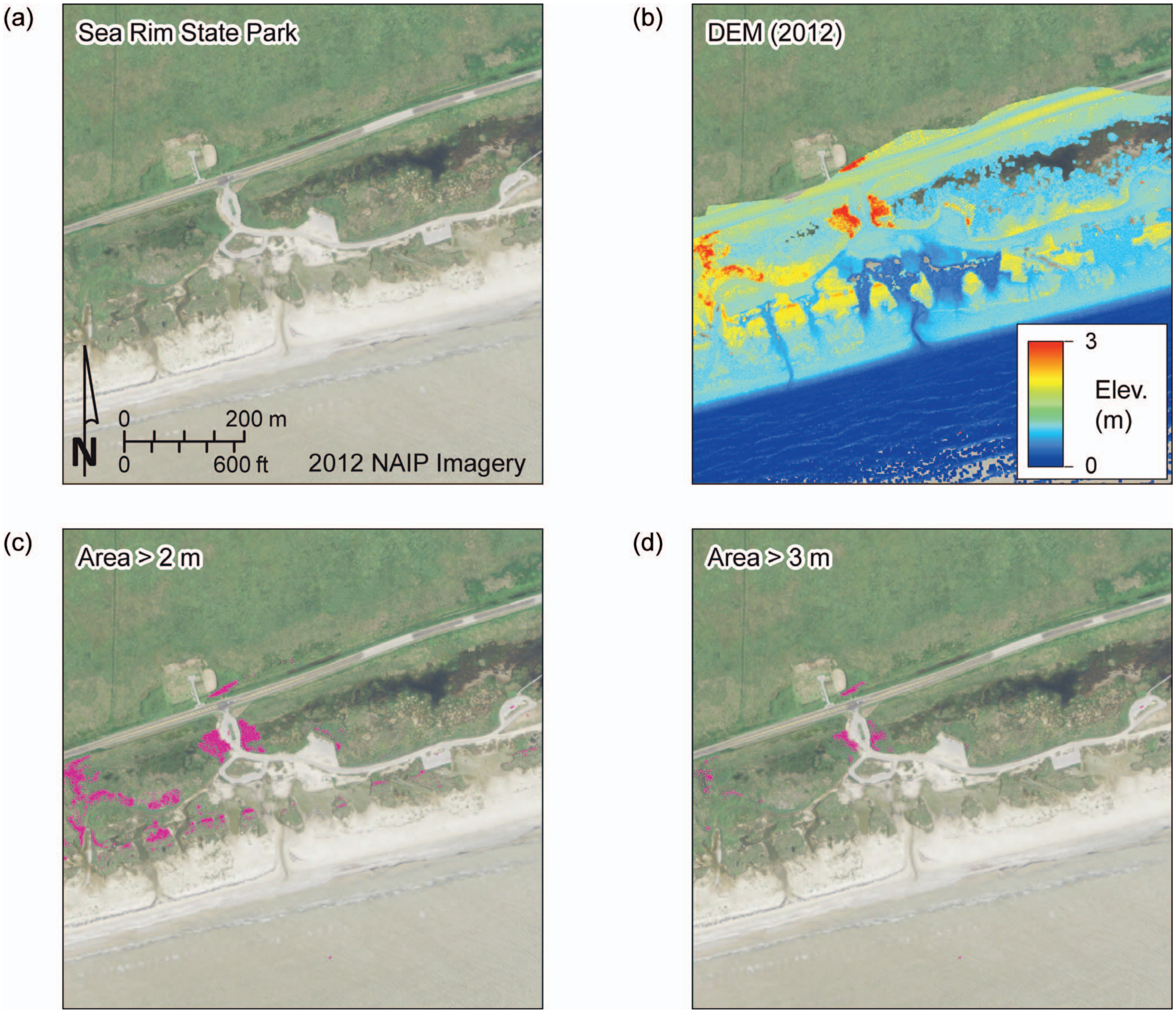

Figure 10. Sea Rim State Park (a) aerial photograph, (b) DEM (2012), and area slices at threshold elevations of (c) 2 m and (d) 3 m on the Sabine chenier plain of the upper Texas coast.

lower normalized areas (or average shore-normal widths) at threshold elevations of 2–5 m.

DISCUSSION

Widespread shoreline advance measured between April 2010 and April 2011 generally counters the historical trend of shoreline retreat along the entire Texas coast (Figures 4, 5, and 13) and the general retreat observed between 2007 and 2010 related to passage of Hurricanes Humberto, Ike, and Dolly. Notable segments of advancing shorelines between 2010 and 2011 included Galveston Island, Follets Island, and the NE part of the Brazos/Colorado headland, and Matagorda Peninsula on the upper coast; most of Matagorda Island and San José Island on the central coast; and the central and southern parts of Padre Island on the lower coast (Figure 5). Significant retreat ($\geq$10 m) was limited to the Sabine chenier plain and Trinity headland, the S flank of the Brazos/Colorado headland and the E part of Matagorda Peninsula, the W end of Matagorda Peninsula and the E end of Matagorda Island at Pass Cavallo, Mustang Island and northern Padre Island, and the shoreline near the mouth of the Rio Grande (Figure 5). Predominant coastwide advance may be attributable to whole-coast recovery from Hurricane Ike during the period from 1.5 to 2.5 y after landfall in September 2008 and to some degree from preceding lesser storms, including Hurricane Humberto (2007) on the upper coast and Dolly (2008) on the lower coast.

Relative trends in coastwide shoreline change between 2011 and 2012 are similar to historical patterns (Figures 4, 6, and

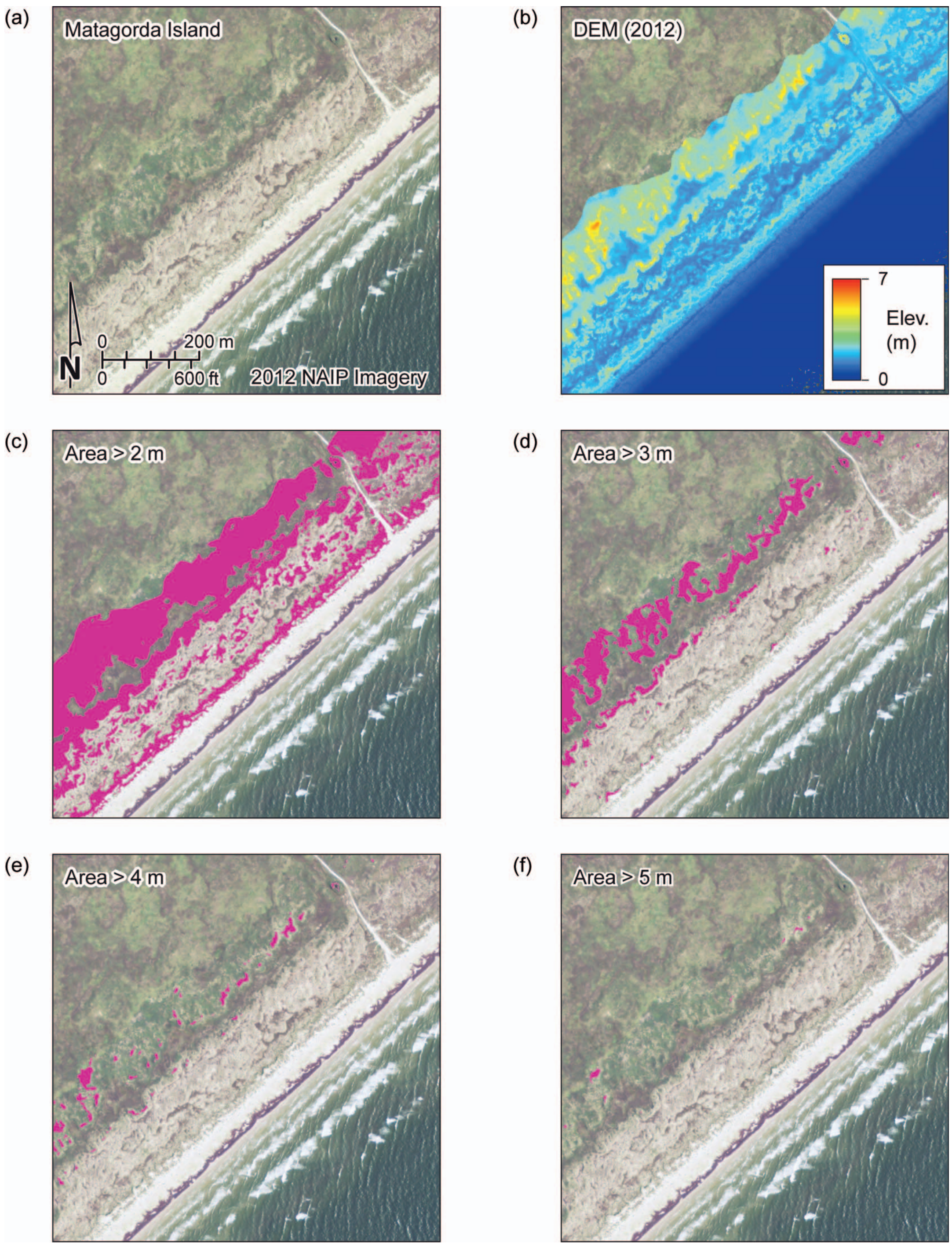

Figure 11. Matagorda Island (a) aerial photograph, (b) DEM (2012), and area slices at threshold elevations of (c) 2 m, (d) 3 m, (e) 4 m, and (f) 5 m on the central Texas coast.

13). Shorelines along the central coast that advanced between 2011 and 2012 coincide with the area that has among the lowest historical erosion rates (retreat at 0.4–1.0 m/y on Matagorda Island, San José Island, and Mustang Island; Figure 4). The southward increase in average retreat along Padre Island between 2011 and 2012 coincides with a similar southward increase in historical retreat rates from northern Padre Island (0.8 m/y) to southern Padre Island (2.3 m/y). Similarly, the increase in average shoreline retreat northeastward from Matagorda Peninsula between 2011 and 2012

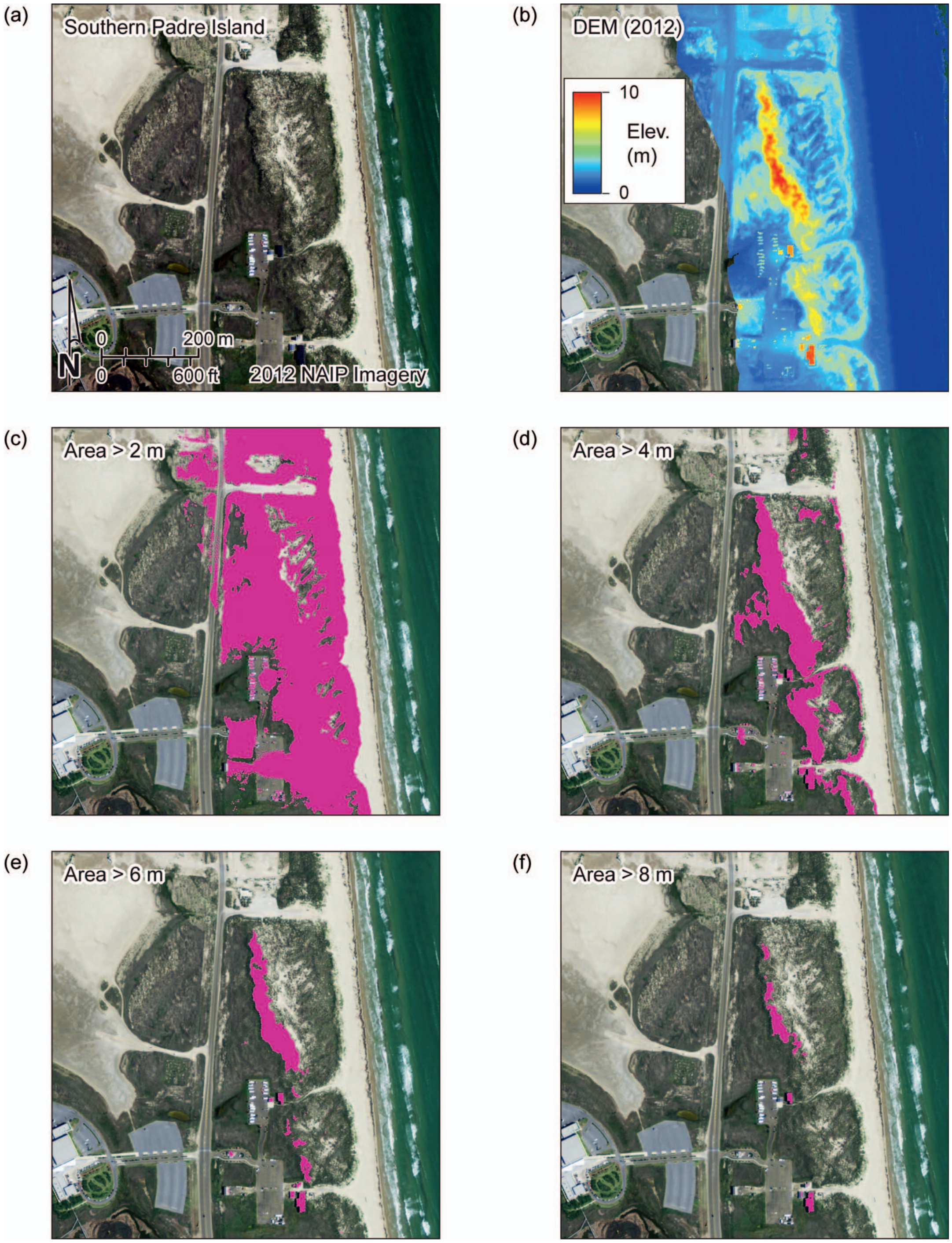

Figure 12. Southern Padre Island (a) aerial photograph, (b) DEM (2012), and area slices at threshold elevations of (c) 2 m, (d) 4 m, (e) 6 m, and (f) 8 m on the lower Texas coast.

mirrors the general northeastward increase in historical retreat rates (excluding Galveston Island and Bolivar Peninsula) to Sabine Pass, including the Trinity headland and Sabine chenier plain. Predominance of shoreline retreat along most of the Texas coast between April 2011 and February 2012 may indicate the end of significant recovery from Hurricanes Ike, Humberto, and Dolly and a return to longer term shoreline change patterns.

Although short-term net coastwide trends measured from 2010 to 2012 generally show shoreline advance (Figures 4, 7,

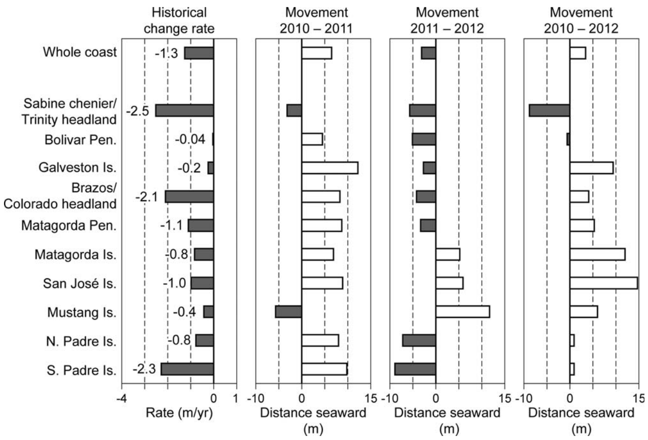

Figure 13. Comparison of incremental shoreline movement measured between 2010 and 2012 with long-term shoreline movement rates along the Texas Gulf shoreline.

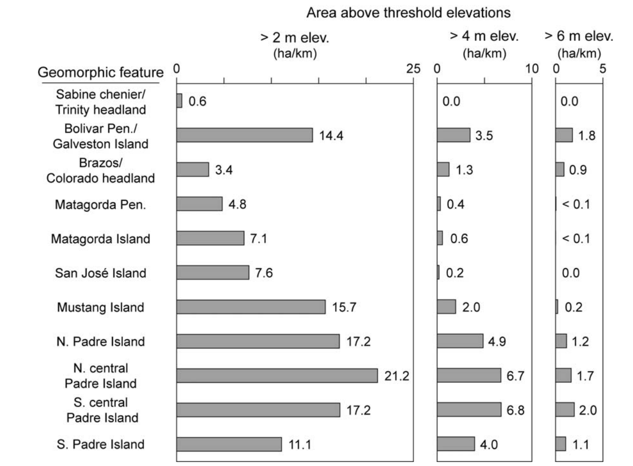

Figure 14. Normalized areas above threshold elevations for major Texas coastal geomorphic features. ETA data calculated from 2012 LIDAR-derived DEMs.

and 13), the relative rates of advance are similar to the historical shoreline change patterns (lesser advance occurs where historical retreat rates are higher; greater advance occurs where historical retreat rates are lower). The greatest amount of shoreline advance between 2010 and 2012 (>10 m; Figure 13) was measured along the central coast between Matagorda Peninsula and Mustang Island, coincident with the segment of the Texas coast where historical average retreat rates are relatively low (0.4–1.1 m/y; Figures 4 and 13). The greatest average amount of shoreline retreat between 2010 and 2012 (~9 m; Figure 13) occurred on the Sabine chenier plain and Trinity headland, where the most rapid historical average retreat rates have been measured (2.5 m/y; Figures 4 and 13). Small average amounts of shoreline advance were measured along Padre Island, where historical patterns indicate moderate to high average rates of erosion.

ETAs calculated from 2012 DEMs for major Texas coastal geomorphic features (Figure 14) show trends along the coast that are similar to historical shoreline movement trends (Figure 13). Geomorphic features having the highest elevation threshold areas per kilometer of shoreline (or greatest average shore-normal widths) at each elevation threshold (Galveston Island and Bolivar Peninsula on the upper Texas coast and Mustang Island and central to northern Padre Island on the lower Texas coast) also experience the lowest historical rates of shoreline retreat (≤0.8 m/y). Conversely, geomorphic features having the lowest elevation threshold areas per kilometer of shoreline at each elevation threshold (Sabine chenier plain, Trinity headland, and the Brazos/Colorado headland on the upper Texas coast; Matagorda Peninsula, Matagorda Island, and San José Island on the central Texas coast; and the southernmost part of Padre Island and the area near the mouth of the Rio Grande on the lower Texas coast) experience the highest historical rates of shoreline retreat (0.8–2.5 m/y). This relationship reveals that areas undergoing chronic shoreline retreat lack large reserves of sand stored in the beach and dune system that could help the local system recover from episodic erosion events such as those that occur during tropical cyclone passage. ETA relationships derived from periodic LIDAR surveys can be used to determine storm surge susceptibility and assess storm recovery potential.

CONCLUSIONS

Three annual airborne LIDAR surveys of the Texas Gulf shoreline were completed in 2010, 2011, and 2012. High-resolution DEMs constructed from the LIDAR data allowed extraction of key coastal features. Short-term shoreline change was determined by comparing annual extracted shoreline position, indicating that shorelines predominantly advanced between 2010 and 2011 during the waning stages of recovery from Hurricanes Ike (2008), Humberto (2007), and Dolly (2008) and then retreated between 2011 and 2012. The 2011–2012 trend is similar to historical shoreline change trends that indicate all major geomorphic features of the Texas Gulf shoreline are retreating at a coastwide average rate of about 1.3 m/y. Nevertheless, retreat between 2011 and 2012 did not fully offset advance between 2010 and 2011. Between 2010 and 2012, the Texas Gulf shoreline advanced at 59% of measurement sites over an average distance of 3.4 m, resulting in a net beach area gain of 203 ha. The overall advance occurred during a period characterized by passage of no significant storms and insignificant relative sea-level rise.

DEMs were used to examine beach and dune land areas above threshold elevations ranging from 2 to 9 m NAVD88. These ETA curves are useful in assessing sand storage patterns, susceptibility to storm surge and erosion, and potential for eventual recovery after episodic erosion events. ETA curves for principal coastal geomorphic features correlate well with historical shoreline change rates: areas with high threshold elevations and large threshold elevation areas are found in relatively stable areas of the Texas coast, whereas areas with low threshold elevations and limited threshold elevation areas are found in places such as the upper Texas coast, where the highest historical retreat rates and frequent surge inundation occur.

ACKNOWLEDGMENTS

This study was supported by grant 09-242-000-3789 from the General Land Office of Texas to the Bureau of Economic Geology, The University of Texas (UT) at Austin under a financial assistance award from the U.S. Department of the Interior, U.S. Fish and Wildlife Service, Coastal Impact Assistance Program. Carly Vaughn (General Land Office) served as project manager. Study support was provided by Jim Reed, Roy Scott, Bob Rodell, David Morgan, Andre Fuegner, and Leonard Laws (Texas Department of Transportation); James Gibeaut, Alistair Lord, and Greg Hauger (Texas A&M–Corpus Christi); Dan Prouty (National Geodetic Survey); and Roberto Gutierrez (UT Center for Space Research). The views expressed herein are those of the authors and do not necessarily reflect the views of the U.S. Fish and Wildlife Service. The manuscript was greatly improved through the efforts of two anonymous reviewers. Publication authorized by the Director, Bureau of Economic Geology.

LITERATURE CITED

Aronow, S.; Fisher, W.L.; McGowen, J.H., and Barnes, V.E., 1982. *Geologic Atlas of Texas, Houston Sheet*. Austin, Texas: The University of Texas at Austin, Bureau of Economic Geology, scale 1:250,000, 1 sheet.

Avila, L.A., 2010. Tropical Storm Hermine (AL102010). *Tropical Cyclone Report*. Miami, Florida: National Oceanic and Atmospheric Administration, National Hurricane Center, 17p.

Balsillie, J.H. and Donoghue, J.F., 2004. *High Resolution Sea-Level History for the Gulf of Mexico since the Last Glacial Maximum*. Tallahassee, Florida: Florida Geological Survey, *Report of Investigations No. 103*, pp. 53–69.

Barnett, T.P., 1983. Global sea level: Estimating and explaining apparent changes. *In:* Magoon, O.T. and Converse, H. (eds.), *Coastal Zone '83, Proceedings of the Third Symposium on Coastal and Ocean Management*. San Diego, California: American Society of Civil Engineers, Volume 3, pp. 2777–2783.

Berg, R., 2009. *Hurricane Ike (AL092008)*. Miami, Florida: National Oceanic and Atmospheric Administration, National Hurricane Center, *Tropical Cyclone Report*, 55p.

Blake, E.S., 2007. *Hurricane Humberto (AL092007)*. Miami, Florida: National Oceanic and Atmospheric Administration, National Hurricane Center, *Tropical Cyclone Report*, 16p.

Brennan, M.J., 2011. *Tropical Storm Don (AL042011)*. Miami, Florida: National Oceanic and Atmospheric Administration, National Hurricane Center, *Tropical Cyclone Report*, 15p.

Brown, L.F., Jr.; Brewton, J.L., and McGowen, J.H., 1975. *Geologic Atlas of Texas, Corpus Christi Sheet*. Austin, Texas: The University of Texas at Austin, Bureau of Economic Geology, scale 1:250,000, 1 sheet.

Brown, L.F., Jr.; Brewton, J.L.; McGowen, J.H.; Proctor, C.V.; Aronow, S., and Barnes, V.E., 1975. *Geologic Atlas of Texas, Beeville-Bay City Sheet*. Austin, Texas: The University of Texas at Austin, Bureau of Economic Geology, scale 1:250,000, 1 sheet.

Brown, L.F., Jr.; Brewton, J.L.; White, W.A., and Owens, F., 1976. *Geologic Atlas of Texas, McAllen-Brownsville Sheet*. Austin, Texas: The University of Texas at Austin, Bureau of Economic Geology, scale 1:250,000, 1 sheet.

Bruun, P., 1954. *Coastal Erosion and Development of Beach Profiles*. Washington, D.C.: U.S. Army Corps of Engineers, Beach Erosion Board, *Technical Memorandum No. 44*, 82p.

Bruun, P., 1962. Sea-level rise as a cause of shore erosion. *Journal of the Waterways and Harbors Division*, 88(1–3), 117–130.

Bruun, P., 1988. The Bruun rule of erosion by sea-level rise: A discussion of large-scale two- and three-dimensional usages. *Journal of Coastal Research*, 4(4), 627–648.

Cazenave, A. and Nerem, R.S., 2004. Present-day sea level change: Observations and causes. *Reviews of Geophysics*, 42(3), 20p. doi:1029/2003RG000139

Church, J.A.; Clark, P.U.; Cazenave, A.; Gregory, J.M.; Jevrejeva, S.; Levermann, A.; Merrifield, M.A.; Milne, G.A.; Nerem, R.S.; Nunn, P.D.; Payne, A.J.; Pfeffer, W.T.; Stammer, D., and Unnikrishnan, A.S., 2013. Sea level change. *In:* Stocker, T.F.; Qin, D.; Plattner, G.-K.; Tignor, M.; Allen, S.K.; Boschung, J.; Nauels, A.; Xia, Y.; Bex, V., and Midgley, P.M. (eds.), *Climate Change 2013: The Physical Science Basis*. Contribution of Working Group I to the Fifth Assessment Report of the Intergovernmental Panel on Climate Change. Cambridge, U.K.: Cambridge University Press, pp. 1137–1216.

Church, J.A. and White, N.J., 2006. A 20th century acceleration in global sea-level rise. *Geophysical Research Letters*, 33(1), 4p. doi:10.1029/2005GL024826

Cooper, J.A.G. and Pilkey, O.H., 2004. Sea-level rise and shoreline retreat: Time to abandon the Bruun Rule. *Global and Planetary Change*, 43(3–4), 157–171.

Emery, K.O., 1980. Relative sea levels from tide-gauge records. *Proceedings of the National Academy of Sciences of the United States of America*, 77(12), 6968–6972.

FitzGerald, D.M.; Fenster, M.S.; Argow, B.A., and Buynevich, I.V., 2008. Coastal impacts due to sea-level rise. *Annual Review of Earth and Planetary Sciences*, 36, 601–647.

Gibeaut, J.C. and Caudle, T., 2009. Defining and mapping foredunes, the line of vegetation, and shorelines along the Texas Gulf Coast. *Final Report Prepared for the Texas General Land Office*. Austin, Texas: The University of Texas at Austin, Bureau of Economic Geology, 14p.

Gibeaut, J.C.; Gutierrez, R., and Hepner, T., 2002. Threshold conditions for episodic beach erosion along the southeast Texas coast. *Gulf Coast Association of Geological Societies Transactions*, 52, 323–335.

Gibeaut, J.C.; Hepner, T.; Waldinger, R.; Andrews, J.; Gutierrez, R.; Tremblay, T.A., and Smyth, R., 2001. *Changes in Gulf Shoreline Position, Mustang and North Padre Islands, Texas*. Austin, Texas: The University of Texas at Austin, Bureau of Economic Geology, *Report of the Texas Coastal Coordination Council and General Land Office Contract 00-002r*, 30p.

Gibeaut, J.C.; White, W.A.; Hepner, T.; Gutierrez, R.; Tremblay, T.A.; Smyth, R., and Andrews, J., 2000. *Texas Shoreline Change Project: Gulf of Mexico Shoreline Change from the Brazos River to Pass Cavallo*. Austin, Texas: The University of Texas at Austin, Bureau of Economic Geology, *Report of the Texas Coastal Coordination Council and General Land Office Contract NA870Z0251*, 32p.

Gornitz, V. and Lebedeff, S., 1987. Global sea-level changes during the past century. *In*: Nummedal, D.; Pilkey, O.H., Jr., and Howard, J.D. (eds.), *Sea-Level Fluctuation and Coastal Evolution*. Tulsa, Oklahoma: Society of Economic Paleontologists and Mineralogists, *Special Publication 41*, pp. 3–16.

Gornitz, V.; Lebedeff, S., and Hansen, J., 1982. Global sea level trend in the past century. *Science*, 215(4540), 1611–1614.

Gutenberg, B., 1941. Changes in sea level, postglacial uplift, and mobility of the Earth's interior. *Geological Society of America Bulletin*, 52(5), 721–772.

Hayes, M.O., 1967. *Hurricanes as Geological Agents: Case Studies of Hurricanes Carla, 1961, and Cindy, 1963*. Austin, Texas: The University of Texas at Austin, *Bureau of Economic Geology Report of Investigations No. 61*, 54p.

LeBlanc, R.J. and Hodgson, W.D., 1959. Origin and development of the Texas shoreline. *Gulf Coast Association of Geological Societies Transactions*, 9, 197–220.

Leuliette, E.W. and Miller, L., 2009. Closing the sea level rise budget with altimetry, Argo, and GRACE. *Geophysical Research Letters*, 36(4), L04608. doi:10.1029/2008GL036010

Leuliette, E.W. and Willis, J.K., 2011. Balancing the sea level budget. *Oceanography*, 24(2), 122–129. doi:10.5670/oceanog.2011.32

Lyles, S.D.; Hickman, L.E., Jr., and Debaugh, H.A., Jr., 1988. *Sea level variations for the United States, 1855–1986*. Rockville, Maryland: U.S. Department of Commerce, National Ocean Service, Office of Oceanography and Marine Assessment, 182p.

McGowen, J.H.; Garner, L.E., and Wilkinson, B.H., 1977. *The Gulf Shoreline of Texas: Processes, Characteristics and Factors in Use*. Austin, Texas: The University of Texas at Austin, *Bureau of Economic Geology Geological Circular 77-3*, 27p.

Milliken, K.T.; Anderson, J.B., and Rodriguez, A.B., 2008. A new composite Holocene sea-level curve for the northern Gulf of Mexico. *In:* Anderson, J.B. and Rodriguez, A.B. (eds.), *Response of Upper Gulf Coast Estuaries to Holocene Climate Change and Sea-Level Rise*. Boulder, Colorado: Geological Society of America, *Special Paper 443*, pp. 1–11. doi:10.1130/2008.2443(01)

Morton, R.A., 1974. *Shoreline Changes on Galveston Island (Bolivar Roads to San Luis Pass), an Analysis of Historical Changes of the Texas Gulf Shoreline*. Austin, Texas: The University of Texas at Austin, *Bureau of Economic Geology Geological Circular 74-2*, 34p.

Morton, R.A., 1975. *Shoreline Changes Between Sabine Pass and Bolivar Roads*. Austin, Texas: The University of Texas at Austin, *Bureau of Economic Geology Geological Circular 75-6*, 43p.

Morton, R.A., 1977. Historical shoreline changes and their causes, Texas Gulf Coast. *Gulf Coast Association of Geological Societies Transactions*, 27, 352–364.

Morton, R.A., 1997. *Gulf Shoreline Movement Between Sabine Pass and the Brazos River, Texas: 1974 to 1996*. Austin, Texas: The University of Texas at Austin, *Bureau of Economic Geology Geological Circular 97-3*, 46p.

Morton, R.A.; Miller, T.L., and Moore, L.J., 2004. *National Assessment of Shoreline Change, Part 1: Historical Shoreline Changes and Associated Coastal Land Loss along the U.S. Gulf of Mexico*. St. Petersburg, Florida: U.S. Geological Survey, *Open-File Report 2004-1043*, 42p.

Morton, R.A. and Paine, J.G., 1985. *Beach and Vegetation-line Changes at Galveston Island, Texas: Erosion, Deposition, and Recovery from Hurricane Alicia*. Austin, Texas: The University of Texas at Austin, *Bureau of Economic Geology Geological Circular 85-5*, 39p.

Morton, R.A. and Paine, J.G., 1990. Coastal land loss in Texas: An overview. *Gulf Coast Association of Geological Societies Transactions*, 40, 625–634.

Morton, R.A.; Paine, J.G., and Gibeaut, J.C., 1994. Stages and durations of post-storm beach recovery, southeastern Texas coast, U.S.A. *Journal of Coastal Research*, 10(4), 884–908.

Morton, R.A. and Pieper, M.J., 1975a. *Shoreline Changes on Brazos Island and South Padre Island (Mansfield Channel to Mouth of the Rio Grande), an Analysis of Historical Changes of the Texas Gulf Shoreline*. Austin, Texas: The University of Texas at Austin, *Bureau of Economic Geology Geological Circular 75-2*, 39p.

Morton, R.A. and Pieper, M.J., 1975b. *Shoreline Changes in the Vicinity of the Brazos River Delta (San Luis Pass to Brown Cedar Cut)*. Austin: Texas: The University of Texas at Austin, *Bureau of Economic Geology Geological Circular 75-4*, 47p.

Morton, R.A. and Pieper, M.J., 1976. *Shoreline Changes on Matagorda Island and San Jose Island (Pass Cavallo to Aransas Pass)*. Austin: Texas: The University of Texas at Austin, *Bureau of Economic Geology Geological Circular 76-4*, 42p.

Morton, R.A. and Pieper, M.J., 1977a. *Shoreline Changes on Mustang Island and North Padre Island (Aransas Pass to Yarborough Pass)*. Austin, Texas: The University of Texas at Austin, *Bureau of Economic Geology Geological Circular 77-1*, 45p.

Morton, R.A. and Pieper, M.J., 1977b. *Shoreline Changes on Central Padre Island (Yarborough Pass to Mansfield Channel)*. Austin: Texas: The University of Texas at Austin, *Bureau of Economic Geology Geological Circular 77-2*, 35p.

Morton, R.A.; Pieper, M.J., and McGowen, J.H., 1976. *Shoreline Changes on Matagorda Peninsula (Brown Cedar Cut to Pass Cavallo)*. Austin, Texas: The University of Texas at Austin, *Bureau of Economic Geology Geological Circular 76-6*, 37p.

Paine, J.G., 1991. Late Quaternary Depositional Units, Sea Level, and Vertical Movement along the Central Texas Coast. Austin, Texas: The University of Texas at Austin, Ph.D. dissertation, 256p.

Paine, J.G., 1993. Subsidence of the Texas coast: Inferences from historical and late Pleistocene sea levels. *Tectonophysics*, 222(3–4), 445–458.

Paine, J.G.; Caudle, T.L., and Andrews, J.R., 2013. *Shoreline, Beach, and Dune Morphodynamics, Texas Gulf Coast*. Austin, Texas: The University of Texas at Austin, *Bureau of Economic Geology Final Report Prepared for General Land Office under Contract 09-242-000-3789*, 64p.

Paine, J.G.; Caudle, T.L., and Andrews, J.R., 2014. *Shoreline Movement along the Texas Gulf Coast, 1930's to 2012*. Austin, Texas: The University of Texas at Austin, *Bureau of Economic Geology Final Report prepared for General Land Office Under Contract 09-074-000*, 52p.

Paine, J.G.; Mathew, S., and Caudle, T., 2011. *Texas Gulf Shoreline Change Rates Through 2007*. Austin, Texas: The University of Texas at Austin, *Bureau of Economic Geology Report Prepared Under General Land Office Contract 10-041-000-3737 and National Oceanic and Atmospheric Administration Award NA09NOS4190165*, 38p.

Paine, J.G.; Mathew, S., and Caudle, T., 2012. Historical shoreline change through 2007, Texas Gulf coast: Rates, contributing causes, and Holocene context. *GCAGS Journal*, 1, 13–26.

Paine, J.G. and Morton, R.A., 1989. *Shoreline and Vegetation-line Movement, Texas Gulf Coast, 1974 to 1982*. Austin, Texas: The University of Texas at Austin, *Bureau of Economic Geology Geological Circular 89-1*, 50p.

Pasch, R.J. and Kimberlain, T.B., 2009. *Tropical Cyclone Report Hurricane Dolly (AL042008)*. Miami, Florida: National Oceanic and Atmospheric Administration, National Hurricane Center, 19p.

Peltier, W.R. and Tushingham, A.M., 1989. Global sea level rise and the greenhouse effect: Might they be connected? *Science*, 44(4906), 806–810.

Penland, S. and Ramsey, K., 1990. Sea-level rise in Louisiana and the Gulf of Mexico: 1908–1988. *Journal of Coastal Research*, 6(2), 323–342.

Price, W.A., 1956. *Hurricanes Affecting the Coast of Texas from Galveston to the Rio Grande*. Washington, D.C.: U.S. Army Corps of Engineers, *Beach Erosion Board Technical Memorandum 78*, 35p.

Roth, D., 2010. *Texas Hurricane History*. Camp Springs, Maryland: National Weather Service, 83p. http://origin.wpc.ncep.noaa.gov/research/txhur.pdf.

Shalowitz, A.L., 1964. *Shore and Beach Boundaries*. Washington, D.C.: U.S. Department of Commerce, *Publication 10-1*, 749p.

Shepard, F.P., 1960. Rise of sea level along northwest Gulf of Mexico. *In:* Shepard, F.P.; Phleger, F.B., and van Andel, T.H. (eds.), *Recent Sediments, Northwest Gulf of Mexico*. Tulsa, Oklahoma: American Association of Petroleum Geologists, pp. 338–344.

Simpson, R.H. and Riehl, H., 1981. *The Hurricane and Its Impact*. Baton Rouge, Louisiana: Louisiana State University Press, 398p.

Snay, R.; Cline, M.; Dillinger, W.; Foote, R.; Hilla, S.; Kass, W.; Ray, J.; Rohde, J.; Sella, G., and Soler, T., 2007. Using global positioning system-derived crustal velocities to estimate rates of absolute sea level change from North American tide gauge records. *Journal of Geophysical Research*, 112, B04409, 11p. doi:10.1029/2006JB004606

Swanson, R.L. and Thurlow, C.I, 1973. Recent subsidence rates along the Texas and Louisiana coast as determined from tide measurements. *Journal of Geophysical Research*, 78(15), 2665–2671.

Thieler, E.R.; Himmelstoss, E.A.; Zichichi, J.L., and Ergul, A., 2009. *Digital Shoreline Analysis System (Dsas) Version 4.0—an Arcgis Extension for Calculating Shoreline Change*. Woods Hole, Massachusetts: U.S. Geological Survey, *Open-File Report 2008-1278*.